Chapter 13
Grinding

13.1 Cutting with Geometrically Undefined Cutting Edges

The process of the group "abrasive processes" or "Cutting with geometrically undefined cutting edges" is structured according to DIN8589-0 (see Sect. 1.2), in the processes grinding with rotating tools, belt grinding, stroke grinding, honing, lapping, free abrasive cutting and abrasive blast cutting (Fig. 13.1). Processes with fixed and loose abrasive particles can be distinguished. These processes are mainly finishing processes. But nowadays, the development of high power grinding processes permits the economic realisation of high material removal rates, so that the areas of application of the processes with a geometrically undefined cutting edge is no longer limited to finishing.

The removal of material can be a path-linked manner (grinding, honing), force-linked (lapping) or energy-linked (blasting). The cutting edges of the abrasive particles are thereby moved tangentially (e.g., in grinding) or normally (e.g., in lapping) to the existing surface (Fig. 13.2). This effective motion determines the effective mechanism: During the *normal* penetration of the single cutting edges material is displaced and as a consequence of these wedge-type, plastic deformations is also tangentially shifted. Several or many such displacement processes [SIM88] in one place, e.g., during lapping, lead to the disruption and separation of material parts. The abrasive particles roll off on the workpiece driven by the lapping wheel and are thereby continuously pressed, normally into the workpiece surface.

When the single cutting edges penetrate *tangentially* e.g., during grinding, the process generally resembles cutting with a geometrically defined cutting edge. In principal, the same separating mechanisms occur during the processes of both groups (Fig. 13.3). In grinding, however, the cutting edges are formed by hard material abrasive particles at which one abrasive particle can have several active cutting edges. In general, the dimensions of the elements involved are considerably smaller than in cutting with geometrically defined cutting edges. Cutting with bond abrasive particles generally occurs with a strongly negative cutting angle. When cutting with rotating tools, the paths of the cutting edges correspond to epicycloids (by means of cutting and feed motions). The form of the cutting

H. K. Toenshoff and B. Denkena, *Basics of Cutting and Abrasive Processes*,
Lecture Notes in Production Engineering, DOI: 10.1007/978-3-642-33257-9_13,

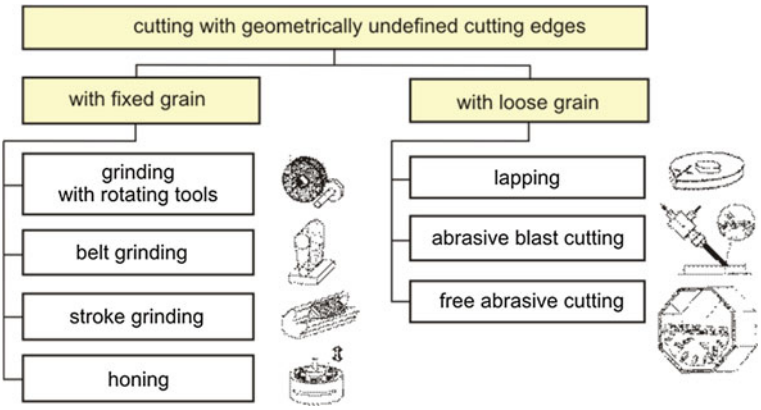

Fig. 13.1 Abrasive processes or cutting with geometrically undefined cutting edges (according to DIN 8589-0)

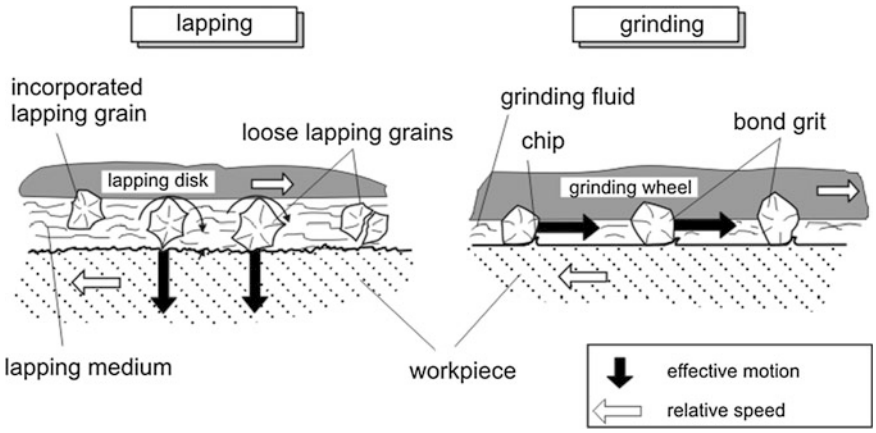

Fig. 13.2 Effective principles and mechanisms during lapping and grinding [SIM88]

wedges and thus the cutting angles, the cutting thickness at each single cutting edge and also the process variables active on the single abrasive particle, such as forces and temperatures, can only be described statistically, e.g., by means of averages, variances and distributions.

The cutting thicknesses during grinding are so small that elastic shares in the deformation are not to be disregarded. Figure 13.4 illustrates the different phases in chip formation. During the cutting edge penetration, after a purely elastic deformation (1), the plastic flow of the material occurs (2). The actual chip formation takes place after another penetration of the cutting edge into the material (3). Apart from the shearing of the chip (4), this area is characterised by elastic as well as plastic deformations. Compared with this, immediately before the abrasive particle leaves the material, there are only elastic deformations and

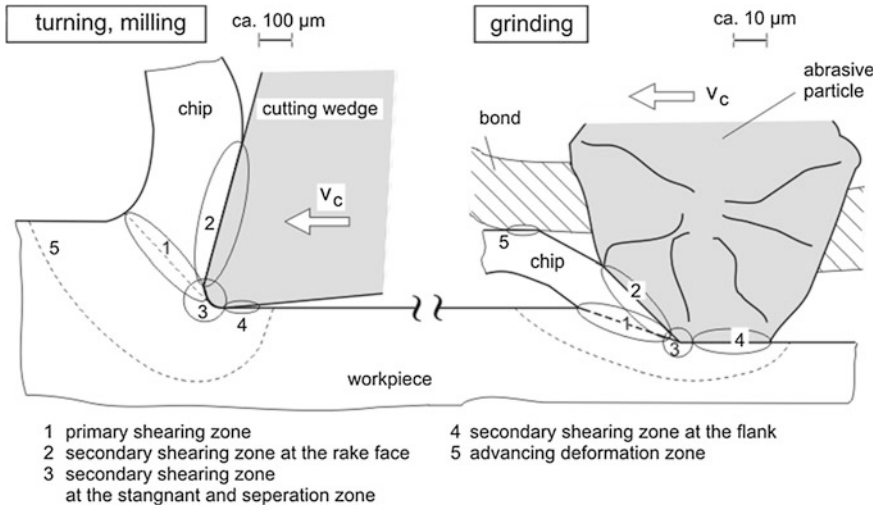

Fig. 13.3 Chip formation

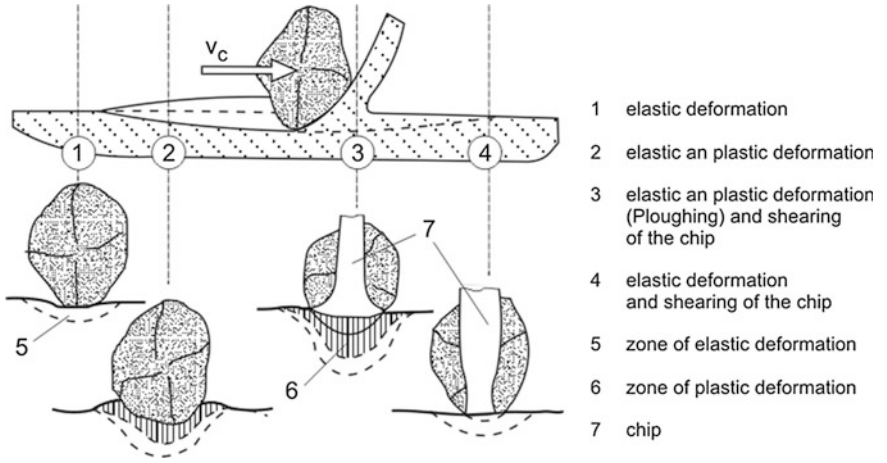

Fig. 13.4 Phases of chip formation during grinding

the shearing of the chip (4). Despite the similarity between grinding and the processes of cutting with geometrically defined cutting edges, several basic differences do exist: In grinding, lateral material flow occurs in front of the cutting edge, the deformation status is triaxial in contrast to a mainly biaxial flow in cutting with a geometrically defined cutting edge [HAH63].

13.2 Grinding Materials

The usual hard materials for grinding are aluminum oxide, silicon carbide, cubic crystalline boron nitride, and diamond. Nowadays, these hard materials for grinding purposes are exclusively produced synthetically, because that way favourable material properties can be reached within tight limits. The grinding materials differ considerably in their degree of hardness and thus in their wear resistance (Fig. 13.5). However, there are also large differences in the other physical characteristics (Table 13.1) [DOW72]. Here, the hardness of diamond has been converted into Knoop resp. Vickers hardness. A direct measurement of diamond hardness is not possible with this process, in fact the hardness is determined indirectly via Young's modulus (E module).

Apart from the hardness, the friability of grinding materials is of interest with regard to the wear behaviour. The friability is determined in a technological—not standardised—process by ball milling coarse grains (particle size 12 US mesh), under determined conditions (ball mass, milling time, etc.,). The process goes back to the "friatester" developed by the company DeBeers [ANSB7418]. The friability index (breakage index) of the grinding material is determined by the proportion of the particles that fall through a mesh with particle size 16 US mesh. Since the process of meshing only uses one mesh width, it is hardly possible to make a statement about the distribution of sizes and thus about the fine friability of interest for the splintering.

In addition, the index numbers for different sizes of abrasive particles are not comparable because smaller sizes generally generate a smaller index number. Friability indices for aluminum oxide of different degrees of hardness were entered in Fig. 13.6 as an example.

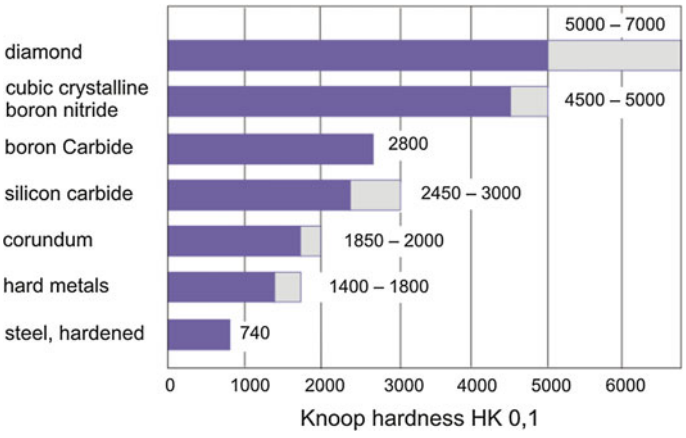

Fig. 13.5 Hardness of abrasives and other materials

Table 13.1 Physical properties of different grinding materials

		Al_2O_3	SiC[1]	CBN	Diamond
Density (g/cm^3)		3.96	3.15	3.48	3.52
Hardness	HK01	1,850–2,000	2,450–3,000	4,500–5,000	5,000–7,000
	HV01	2,100	2,500	6,000	
Young's modulus (GPA)		400	400	680	890
Poisson ratio(−)		0.2	0.17	0.17	0.2[4]
Friction co-efficient (−)		0.34	2.300	0.19	0.05–0.15[4]
Melting point (°C)		2,050		2,730	3,700
Temperature stability (°C)		1,750	1,500	1,200	900
Heat expansion co-efficient (10^{-6}/K)		7.4(<500 °c) 7.5–8.5 (>500 °c)	4.7	3.6	0.8 (RT)[4] 1.5–4.8 (>500 °C)
Heat conductivity (W/mK)		30 (RT) 14 (400 °C)	110 (RT)[2] 55 (600 °C)	200 (400 °C)[3]	600–2,000 (RT)[4]
Related heat (J/gK)		1.08 (400 °C)	1.1 (500 °C)	1.57 (400 °C)[3]	6.19 (RT)[4]

Source 1 Saint Gobain Abrasives; *2* Salmang, Scholze; *3* De Vries; *4* Element Six

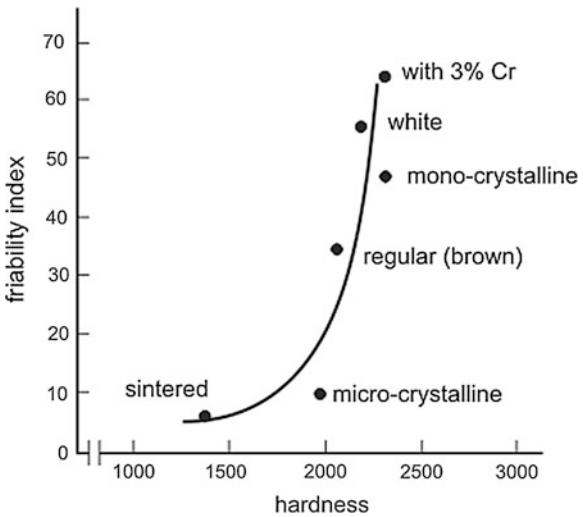

Fig. 13.6 Friability index and hardness, according to Malkin [MAG08]

13.2.1 Corundum

Corundum is a crystalline aluminum oxide (also called alumina) (Al_2O_3). The mechanical properties are determined by the purity degree to a large extent. We differentiate between regular or brown, white and modified aluminum oxide.

In the production of corundum, bauxite serves as a raw material for all qualities, a mixture of different aluminum oxide hydrates which is polluted with ferric hydroxides, silicates and titanium alloys [SAL82]. In the most frequently used Bayer process, ground bauxite with an Al_2O_3 content of 55–60 % is treated with caustic lye at approx. 250 °C under a pressure of 4 MPa. The aluminum oxide

hydrates dissolve as sodium aluminate, the pollutions are separated as so-called red mud. The sodium aluminate lye is stowed with finely dispersed aluminum hydroxide, which as a crystallisation seed, leads to the growth of $Al(OH)_3$ crystals. The calcination of the aluminum hydroxide in fluidised-bed furnaces at 1,200–1,300 °C produces Al_2O_3 (alumina) [SAL82].

Melting the alumina in an electric furnace at temperatures of approx. 2,000 °C generates corundum (Al_2O_3). With this process, it is possible to obtain a high purity degree. The sizes of abrasive particles required for the grinding materials are produced by means of controlled crushing in crushers. Chemical post-treatment process by means of calcination and washing in lyes and acids lead to an improved surface structure of the abrasive particles and targets an increase in their adhesion within the bond.

A very fine original abrasive particle is obtained by means of the s*ol-gel process*, which emanates from a liquid or easily soluble compounds. The sol-gel process allows the production of ceramic and glassy compounds at low temperature. The process is characterised by the changeover of a liquid or colloidal solution (smallest particles of the dimension 10^3–10^4 atoms, mixed with molecules of the solvent) into a solid gel.

For the production of Al_2O_3 with the sol–gel process, a solution of aluminium and an organic ester ($Al(OC_3H_7)_3$) is hydrolysed with H_2O and then condensed under dehydration, which generates a very fine gel well suitable for sintering.

A performance increase of corundum grinding materials can be obtained by altering the structure and shape of the abrasive particles (Fig. 13.7). During the grinding process, the number of sharp cutting edges per abrasive particles can be increased, thus improving the tool life and the power conversion compared with untreated melted corundum. On the other hand, an increase in wheel porosity at

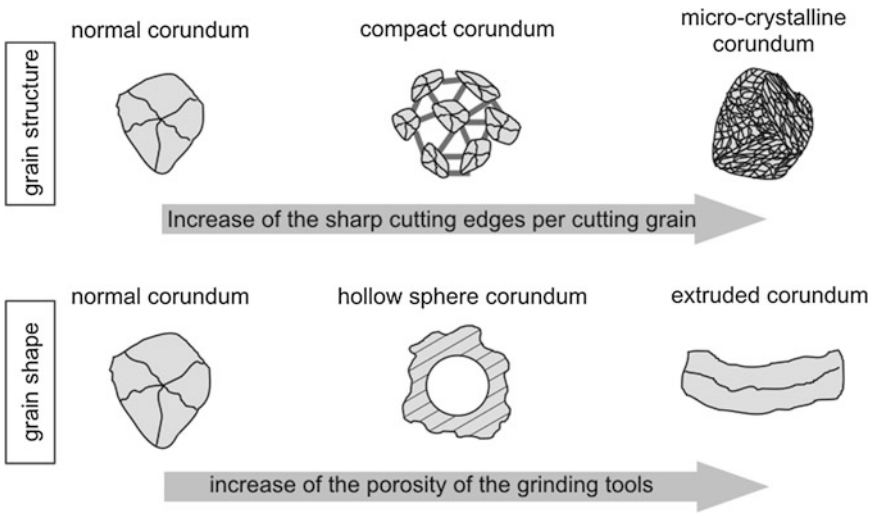

Fig. 13.7 Possibilities of power increase when using aluminum oxide

unaltered wheel strength allows an easier removal of the chips from the effective zone. In addition, the feed of cutting fluid to the contact zone is better at an increased wheel porosity.

During the grinding process, suitably distributed abrasive particles may wear to such a degree that extensively sharp cutting edges are generated. This resharpening or self-sharpening process can be obtained by using compact abrasive particles or particles with a micro crystalline structure. The compact abrasive particles consist of a multitude of small grains, which have been clinkered into a large abrasive particle by means of a bond. The process-related wear on each small grain leads to a local increase in the specific grinding force on the worn abrasive particle. When the bonding forces are surpassed, the blunt abrasive particle detaches itself from the compound of the compact abrasive particle and exposes a new sharp abrasive particle located underneath. This type of resharpening process of abrasive particles is preferably used for abrasives on backing materials, e.g., belt grinding processes [ARG00].

Resharpening is also transferable to each single grain by producing micro crystalline Al_2O_3 according to the sol-gel process. At this, grain fracture and thus sharp cutting edges can occur during the grinding process. In contrast with the coarsely crystalline melting corundums, this mechanism leads to a considerably reduced wear with decreased grinding force and temperature at the same time. This results in longer wheel life, longer dressing intervals and allows an increase of the material removal rate [UHL87, BRU98, MÜL01]. At this, different micro crystalline corundums differ considerably in the height of the initial force required for resharpening [STA02].

In grinding processes with a high material removal rate, grinding wheels with high pore proportions are applied. The maximum porosity readily accounts for about 50 %. A further increase leads to a lower strength, which limits the maximum cutting speed and increases the wear rate. By inserting hollow ball corundum, a hollow corundum grain, into the grinding wheel structure, the porosity can mount to 60 % [MAH00]. Special machining processes can produce grains with large length/diameter relations (aspect ratio) of up to 8. In comparison, the normal corundum grain has an aspect ratio of 1. An advantage of elongated particles is the extension and improvement of the natural packing porosity of the particles. Grinding wheels with a porosity of up to 80 % can be produced without artificial pore builders.

13.2.2 Silicon Carbide

Silicon carbide is one of the important ceramic materials. It is also used as a grinding material. The technical production of SiC takes place according to the *Acheson process* from quartz sand (SiO_2) and petrol coke at a temperature of 2,000–2,300 °C after the stoichiometric reaction

$$SiO_2 + 3\ C \rightarrow SiC + 2\ CO. \quad (13.1)$$

At this, the reactions also occur via intermediate reactions following the presence of gasiform silicon and carbon compounds. The silicon carbide gained by means of the Acheson process occurs at a purity of 98–99 %. The pollutions (Fe, Mg, Ca) are accumulated at the grain edges or in the pores. The material is crushed, cleaned and separated by meshes according to the particle sizes. A multi-step washing process allows the cleaning of the SiC. An acid treatment loosens existing iron residues. Free silicon and silicon compounds are separated with soda lye and graphite with water.

The colour allows the differentiation of the two qualities of SiC, which are characterised by their chemical composition. Black SiC ($\approx$98 %) compared to green SiC ($\approx$99.5 %) shows greater pollutions of free carbonate and elements such as Fe, Al, Ca, Mg and free silicon. The pollutions show no influence on the hardness. However, the ductility of black SiC is higher than that of green SiC.

13.2.3 Cubic Crystalline Boron Nitride and Diamond

Grinding materials made of cubic crystalline boron nitride, also called Cubic Boron Nitrides (CBN) and diamond are extremely hard grinding materials, which are summarised under the term "superabrasives" in English language use. The structure and production process are illustrated in Chap. 8 [BUN55, HAL60]. While the production of CBN is only synthetic, diamond can be differentiated into natural and synthetic. As grinding materials in grinding wheels, exclusively synthetic diamond is used nowadays. CBN has a cubic face centred crystal lattice of nitrogen and boron atoms similar to diamond, which also has a cubic face centred lattice with four additional carbon atoms [KEL80]. Different crystal forms can occur due to the different sliding planes (Fig. 13.8). For synthetic diamond, these range from the octahedron (111 plane) to the cube (100 plane). The diamond is anisotropic, e.g., the hardness is higher in the 111 plane than in the 100 plane [RAM78]. Because of the slightly different crystal structure, CBN crystals can take up further shapes from the octahedron to the tetrahedron.

Due to their crystal structure, the grains contain cleavage planes, which they preferably split along. During the grinding, the abrasive particles blunt. Thus, they are loaded more strongly and split. This generates new cutting edges, which is called self-sharpening. According to the type and number of cleavage planes, one can differentiate mono, macro and micro crystalline structures.

Diamond is the hardest known material. In connection with its high wear strength, it is predestined for the use as a cutting material for the machining of hard materials such as glass, hard metal and ceramic. However, at temperatures above 650 °C in the air, diamond transforms into the energetically more convenient modification of graphite with iron and nickel acting as catalysts and shifting the transformation point to lower temperatures [MAR01]. Carbon also shows a high

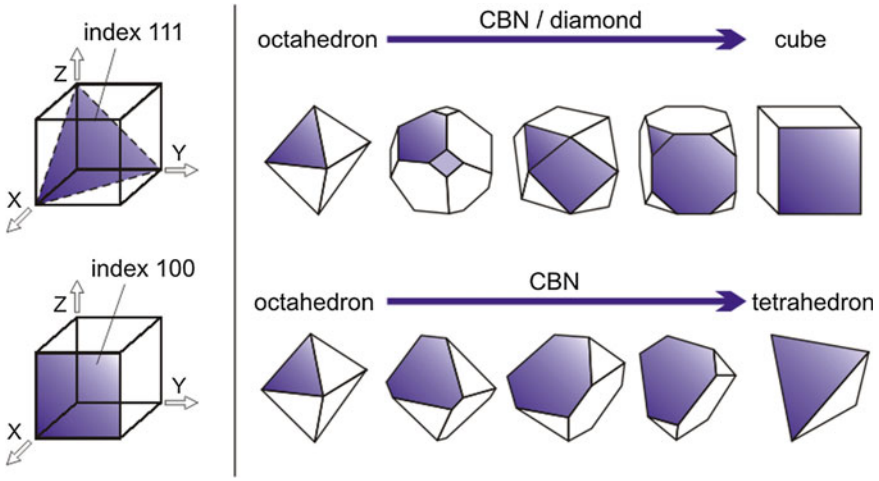

Fig. 13.8 Possible crystal forms of CBN and diamond (*Source* Element six)

affinity to iron so that chemical wear occurs at higher temperatures—thus at higher cutting speeds. Both effects, the graphitisation and the chemical wear lead to the fact that diamond is not used as a grinding material for the machining of steel materials. In contrast, CBN shows no reaction of this kind and is stable at an atmospheric pressure of up to a temperature of 1,400 °C and thus suitable for the machining of ferrous workpieces.

The friability test is a recognised method for the strength determination of diamonds. It is based on the measurement of the impact strength of a defined number of diamonds of a certain abrasive particle size. The number of diamonds that resist the "crushing effort" is a measure for the strength of the examined type of diamond (TI) (also see Sect. 13.2). To determine their thermal stability, diamonds are thermally loaded under protective gas at 1,100 °C for 20 min and then again submitted to the friability test (TTI). The difference between the strength before and after the thermal load is a measure for the thermal stability of the material. This thermal stability is relevant for the application of the tool, but also in the manufacturing of a grinding wheel by sintering [VOL00].

13.2.4 Grain Sizes of Grinding Materials

Abrasive particles are characterised by physical properties, such as hardness, elastic modulus, density, heat conductivity and heat capacity but also by geometrical properties, such as grain size and grain shape. The abrasive particle size in grinding materials from aluminum oxide and silicon carbide up to grit size 220, which corresponds to a medium abrasive particle diameter of about 58 µm, results

sieve grit sizes				
Europe (metrical) (1)	(2)	sieve mesh width in µm	USA (mesh) (1)	(2)
1181	1182	1180 - 1000	16 / 18	16 / 20
1001		1000 - 850	18 / 20	
851	852	850 - 710	20 / 25	20 / 30
711		710 - 600	25 / 30	
601	602	600 - 500	30 / 35	30 / 40
501		500 - 425	35 / 40	
426	427	425 - 355	40 / 45	40 / 50
356		355 - 300	45 / 50	
301	-	300 - 250	50 / 60	-
251	252	250 - 212	60 / 70	60 / 80
213		212 - 180	70 / 80	
181	-	180 - 150	80 / 100	-
151	-	150 - 125	100 / 120	-
126	-	125 - 106	120 / 140	-
107	-	106 - 90	140 / 170	-
91	-	90 - 75	170 / 200	-
76	-	75 - 63	200 / 230	-
64	-	63 - 53	230 / 270	-
54	-	53 - 45	270 / 325	-
46	-	45 - 38	325 / 400	-

Fig. 13.9 Classification system for abrasive particle sizes of super hard grinding materials (according to FEPA[1])

from meshing. For this, standardised wire sieves are used [DIN ISO8486-1]. Due to the heterogeneous grain shapes, there is a statistic distribution of the abrasive particle diameter after meshing, so a classification of the permitted deviations was carried out. This classification is standardized by the FEPA.[1] A grain mixture, for example generated by crushing and milling, is routed to increasingly tighter aperture by means of sieves. In the case of aluminum oxide and silicon carbide, the grain size is defined by the number of meshes per inch of the meshing sieve at a determined wire diameter. A grit size of 60 is removed from the grain compound with a sieve of 60 meshes per inch, which corresponds to a mesh distance of 0.42 mm. Grain sizes finer than 220 are determined by optic sedimentation from a suspension. The sieve analysis entails that the abrasive particles occur in fractions with typical distributions, which also depend on the grain shape.

The super hard grinding materials diamond and CBN are marked according to the clear mesh width of the sieves, i.e., the index correlates directly with the grain diameter. Figure 13.9 contrasts the classification system used in Europe with the US system (mesh). To extend the field of tolerance, one can differentiate between a narrow (1) and a wide dispersion area (2). Both systems are only defined up to a medium grain diameter of $d_g = 46$ µm. Smaller grain sizes are defined by the producers of grinding materials themselves.

[1] FEPA: Federation Europeene des Fabricants de Produits Abrasifs—Federation of European Producers of Grinding Materials.

13.3 Bonding

The abrasive particles are bonded by bonding materials or bonds in the grinding tool. The most important bonds are vitrified bonds, synthetic resinoid and metal bonds.

Vitrified bonds consist of kaolin, clay, quartz, feldspat and flux material [KLO86, PAD93, COL81]. Magnesium oxide or borosilicate containing glasses are used as flux materials to reduce the calcination temperature. The charges fired together with the abrasive particles to grinding tools, at temperatures of 1,100–1,400 °C maximum for corundum and silicon carbide wheels, below 1,000 °C for boron nitride and below 700 °C for diamond. The choice of the charge materials allows the attainment of melting with different viscosity and surface tension. Thus, the structure resp. the porosity of the vitreous-bound grinding wheels can be adjusted.

Synthetic resinoid bonds mainly consist of thermosets, i.e., phenolic resin or compounds with phenolic resins with other resins. They are converted into grinding tools together with the abrasive particles by means of hot pressing. The pressing temperatures are between 150 and 170 °C.

Metal bonds are produced by pressing and sintering bronze, steel or hard metal powders or applied by the galvanic coating with nickel or nickel compounds. Bonds created on the basis of metal powder are sintered under pressure at temperatures of 700–900 °C. Metal bonds are applied for extremely hard grinding materials. They offer a good heat removal from the active grinding layer, have good form stability and show a high adhesion to the abrasive particles. They are often used for profile grinding. Electro-plated grinding wheels mostly feature only one grain layer and are generally not dressed (see Sect. 13.5). By crushing (pressing), dressable metal bonds have been developed by means of inserting brittle fillers.

Other bonding materials are employed for special purposes, e.g., mineral bonds (silicate, magnesite bonds), glue or rubber bonds. The *rubber bond* based on synthetic rubber is used for especially temperature-sensitive processing tasks (knife sharpening), for example.

An important characteristic of a grinding tool is its hardness, which is determined as the resistance opposed by the bond to the quarrying out of abrasive particles. Thus, the hardness of a grinding wheel is basically defined other than usual, since generally the hardness of indentation is determined. The hardness of the wheel or bond is of great relevance for the grinding process. It determines how long a worn abrasive particle is kept in the bonding formation. A soft bond releases abrasive particles at an early stage; the grinding wheel remains sharper compared with a wheel with a hard bond. The practical rule resulting from this: soft, less wearing materials are processed with hard wheels and hard materials with soft wheels. Harder wheels are also recommended for low chip thicknesses, i.e., in short contact lengths or low speed conditions.

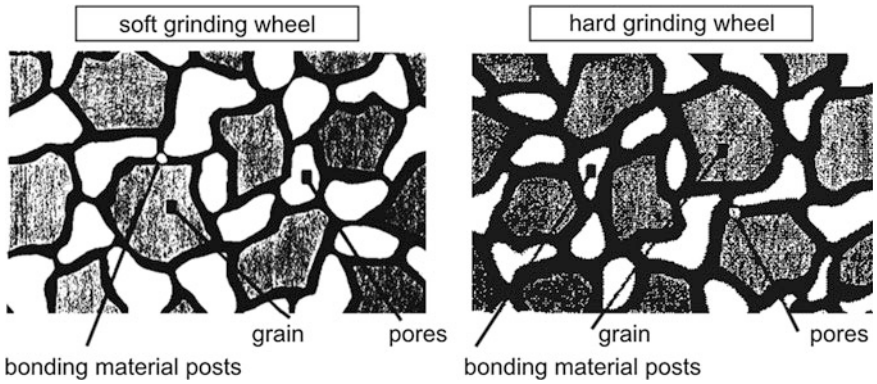

Fig. 13.10 Structure of a vitrified grinding wheel (*Source* "Saint Gobain Abrasives")

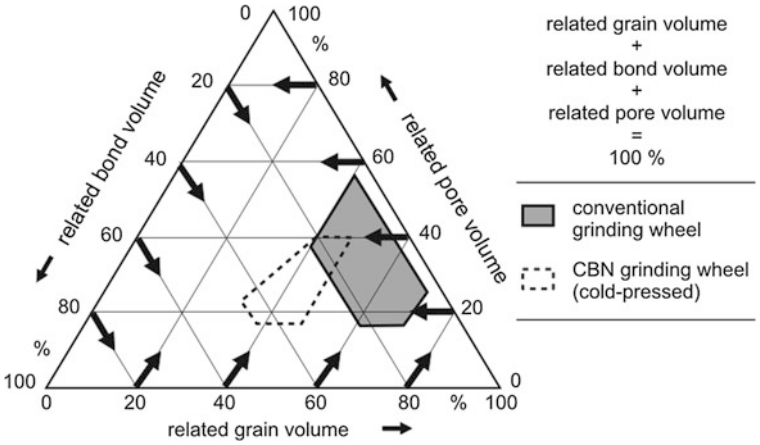

Fig. 13.11 Volume shares of vitrified grinding wheels

For vitrified-bond grinding wheels, the hardness is mainly determined by the abrasive particle size and the thickness of the bonding bridges (Fig. 13.10). Stronger bonding bars maintain the abrasive particles within the structure more strongly and thus provide a higher degree of hardness of the grinding wheel. Figure 13.11 illustrates the areas of common configurations for grinding wheels.

13.4 Grinding Wheels

The material classification of conventional grinding wheels takes place according to [DIN ISO 525] (Fig. 13.12). It contains eight codes including two free codes, i.e., they can be freely chosen by the producer.

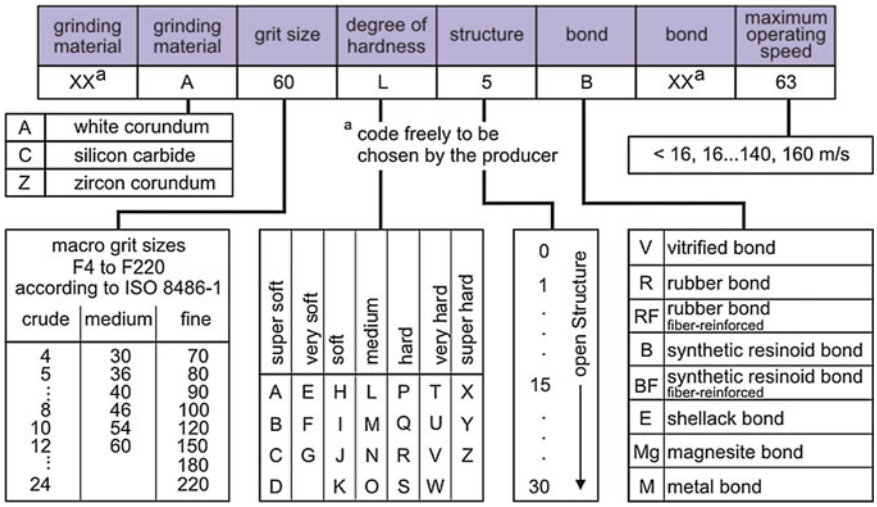

Fig. 13.12 Classification of corundum and silicon carbide grinding wheels (according to DIN ISO 525:2000)

The hardness of a grinding wheel is classified according to the Norton scale with code letters from A (extremely soft) to Z (super hard). The area from E and G (very soft) till P and S (hard) is actually used in practice.

The manual scratch test with a stylus and the comparison with known wheels is subjective and offers no absolute data. A variant of this manual test developed for research purposes is the scratch test according to Peklenik [PEK57], at which a scratching tool is pulled over the surface of the active grinding wheel surface under defined normal load and abrasive particles or parts of them break off in this test. The emerging tangential forces are a measure for the hardness of the wheel. This test comes as close as possible to the definition of hardness, however it is not suitable as a shop testing process.

The hardness test of grinding wheels by means of the shot blasting process according to C. Zeiss and M. Mackensen (tester of Mengringhausen company, Iserlohn) is defined in guideline 102 of the German Grinding Wheel Committee. In this process, a defined volume of a certain sand grit is blown onto the surface of the grinding wheel with pressurised air at a determined static pressure and defined blast cross-section. Figure 13.13 illustrates the structure of a blast tester. The depth of the developing calotte, the so-called blowing depth, is consulted as a measure for the hardness of the grinding wheel. A disadvantage of this process is that it does not work without damage and that the kind of load on the abrasive particles and the bonding is not identical with the hardness definition.

Concerning the load, it is similar to the crushing process (Fig. 13.14). At this, a steel wheel with defined pressure is pressed against the grinding wheel to be tested. Grinding wheel and roller roll against each other. The rolling depth reached after a certain number of rotations is correlated with the wheel hardness. From the

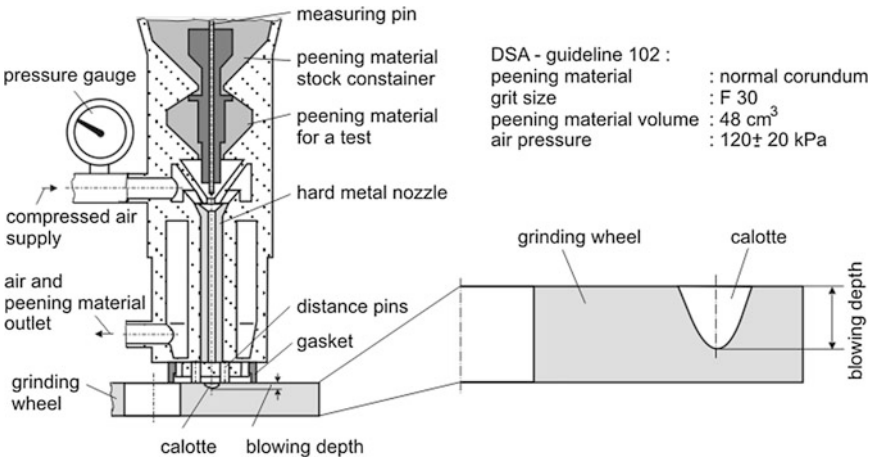

Fig. 13.13 Hardness test of grinding wheels by determination of the blowing depth

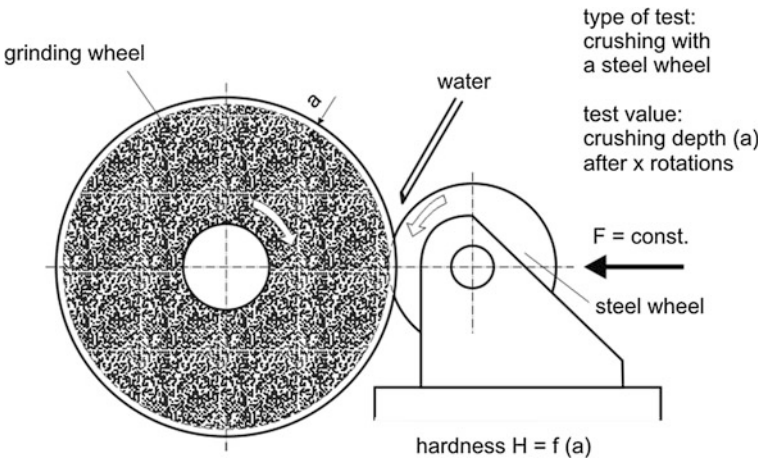

Fig. 13.14 Grinding wheel hardness test according to the rolling process (*Source* Opitz)

perspective of the load on abrasive particles and bonding, the hardness test B according to Rockwell (ball groove test), which mainly tests very fine-grained grinding tools (honing and oil stone tools), is comparable with the rolling process.

A test process, which provides a physical value, is the eigenfrequency measurement (grindo-sonic process) according to R. Snoeys [PET68]. At this, the first eigenfrequency of the grinding wheel is determined by striking in the attenuation test (Fig. 13.15). The eigenfrequency is proportional to the root of the apparent E module of the grinding wheel. With the diameter of the wheel d_a and the hole d_i, the wheel thickness b_s, the average (apparent) density ρ_s and the Poisson's ratio ν,

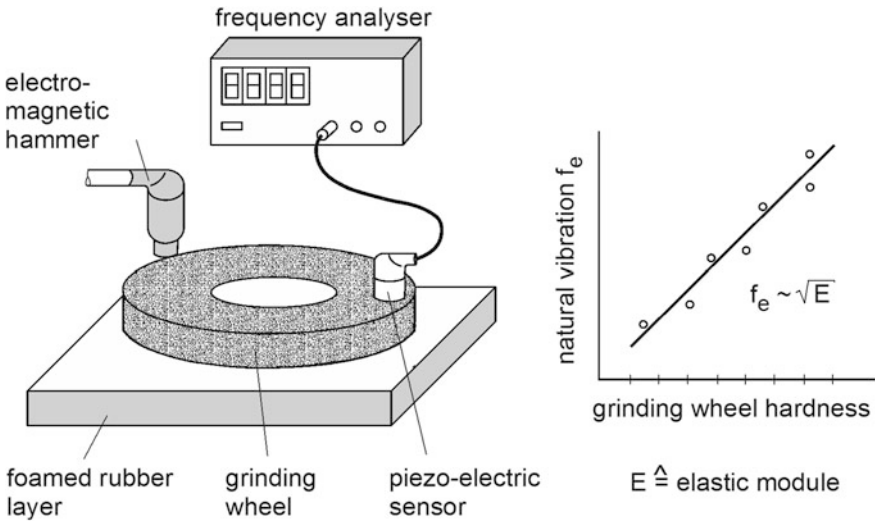

Fig. 13.15 Grinding wheel hardness and E module

the following is valid for the eigenfrequency f_e of the natural oscillation with three node diameters under the condition $d_i/d_a < 0.25$ [PET68]:

$$f_e = \frac{b_s}{d_a^2} \cdot \left(\frac{1 - (d_a/d_i)^2}{1.07(1 - \nu^2) \cdot \rho_s} E \right)^{1/2} \tag{13.2}$$

The specimen, which consists of several components, can be described only as an apparent E module. The thicker the bonding bars, the bigger the E module. This provides a correlation between the E module determined that way and the hardness of the wheel.

The testing process of conventional grinding wheels is transferable to super hard grinding wheels only to a limited extent. There are first method approaches to do determine the fracture behaviour (bonding, abrasive particle) resp. the compliance of super hard vitrified-bound grinding wheels. They apply test loads to single abrasive particles [KLO02] or groups of abrasive particles with a defined tester [DEN03].

13.5 Burst Safety of Grinding Wheels

Grinding wheels run at high circumferential speeds. As a consequence, they are submitted to high radial accelerations, which in turn cause high stress through the centrifugal effect. These stresses can lead to the destruction of the grinding wheels, which is to be avoided. So the loads as a result of the centrifugal forces and their parameters of influence have to be determined.

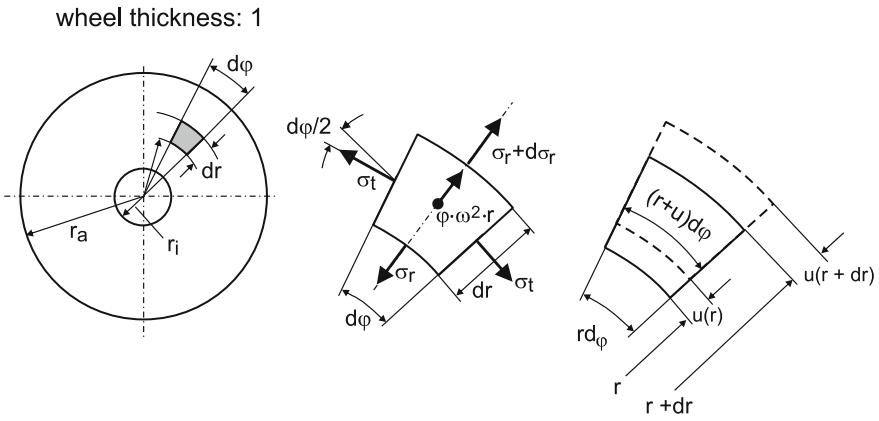

Fig. 13.16 Stresses and strains on the volume element

Figure 13.16 shows stresses and strains on the volume element of a wheel. Due to the low extension vertically to the drawing plane, biaxial stress condition can be presumed. From the balance of the forces in radial direction, it can be written

$$\left(\sigma_r + \frac{\partial \sigma_r}{\sigma r} dr\right) \cdot (r + dr) d\varphi \cdot 1 - \sigma_r \cdot r \cdot d\varphi \cdot 1 - 2 \cdot \sigma_t \cdot dr \cdot 1 \cdot \sin\frac{d\varphi}{2} + \rho \cdot r^2 \cdot \omega^2 \cdot dr \cdot d\varphi = 0 \tag{13.3}$$

In addition, the following is valid for small sections

$$\sin\frac{d\varphi}{2} = \frac{d\varphi}{2}$$

So in summary, it can be written

$$\frac{\partial(\sigma_r \cdot r)}{\partial r} \cdot dr \cdot d\varphi - \sigma_t \cdot dr \cdot d\varphi + \rho \cdot r^2 \cdot \omega^2 \cdot dr \cdot d\varphi = 0 \tag{13.4}$$

A link between σ_r and σ_t is obtained using the material law for elastic behaviour, the Hook's law. As shown in Fig. 13.16, the strains result from the displacements u in radial direction.

$$\varepsilon_r = \lim_{\Delta r \to 0} \frac{u_{r+\Delta r} - u_r}{\Delta r} = \frac{\partial u}{\partial r} \tag{13.5}$$

and

$$\varepsilon_t = \frac{2\pi(r + u) - 2\pi r}{2\pi r} = \frac{u}{r} \tag{13.6}$$

The Hook's law for the plane stress conditions adds up to:

$$\varepsilon_r = \frac{1}{E}[\sigma_r - \nu \cdot \sigma_t] \text{ and}$$

$$\varepsilon_t = \frac{1}{E}[\sigma_t - \nu \cdot \sigma_r] \tag{13.7}$$

which finally results in the differential equation, solvable by means of two-fold integration:

$$\frac{d}{dr}\left[\frac{1}{r} \cdot \frac{d}{dr}(u \cdot r)\right] = -\frac{\rho \cdot (1 - \nu^2)}{E} \cdot r \cdot \omega^2 \tag{13.8}$$

The following solutions result with the boundary conditions for the force-free edges and the (for a dimension-free illustration) radiuses $Q = r/r_a$ and $Q_i = r_i/r_a$ related to the external radius r_a

$$\frac{\sigma_r}{\rho \cdot r_a^2 \omega^2} = \frac{3 + \nu}{8}\left(1 + Q_i^2 - \frac{Q_i^2}{Q^2} - Q^2\right) \tag{13.9}$$

$$\frac{\sigma_t}{\rho \cdot r_a^2 \omega^2} = \frac{3 + \nu}{8}\left(1 + Q_i^2 + \frac{Q_i^2}{Q^2} - \frac{1 + 3\nu}{3 + \nu}Q^2\right) \tag{13.10}$$

Figure 13.17 shows that the maximum load of a grinding wheel occurs as a consequence of centrifugal forces at the internal edge. In fact, wheels, which are operated above their burst speed, are dispersed into segments with radial breaking faces.

For a full wheel, which would then be held to a holding adapter [GRE58] for example, a totally different stress course results theoretically (holelessness). In Eqs. 13.9 and 13.10, the following limit has to be generated according to the law by de L'Hospital:

$$\lim_{Q \to 0} \frac{Q_i^2}{Q^2} = 0 \tag{13.11}$$

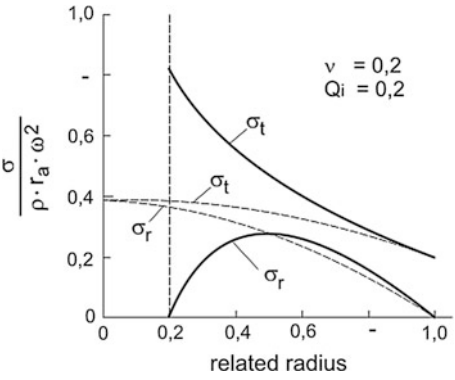

Fig. 13.17 Radial and tangential stresses through centrifugal forces

Thus, the stresses in the centre of the wheel become $Q = Q_i = 0$

$$\frac{\sigma_r}{\rho \cdot r_a^2 \omega^2} = \frac{\sigma_t}{\rho \cdot r_a^2 \omega^2} * = * \frac{+\nu}{\circ} \tag{13.12}$$

In Fig. 13.17, the stress course of a full wheel has been entered in a dotted way. It is recognisable that the tangential and radial stresses in the middle change discontinuously compared with the holed wheel. They are equal, the tangential stress reduces to half of the value of the holed wheel. However, it remains questionable whether "holelessness" can actually be assumed in a porose wheel such as in a vitrified bound one.

The bursting is critical, especially in the case of vitrified bound wheels. In contrast to this, the trend is to increase the grinding speed. The following measures are suitable to increase the burst rpm of the grinding wheel:

- Fitting of reinforcements in the highly-loaded zones (stronger bonds, fiber reinforcement).
- Insertion of a steel ring into the wheel hole and creation of a pull-loadable connection, e.g., by gluing.
- Dissolving the wheel into segments, who do not transfer tangential stresses; however, this requires a safe radial clamp of the segments.
- Double-cone-shaped construction of the wheel so that the stress is reduced against the internal edge.

Due to the high energy content of the grinding wheels or their fragments at high grinding speeds (the speed effects in the 2nd order), special safety requirements are to be observed. In grinding machines (stationary machines), only grinding wheels authorised according to DIN ISO 13236 and according to DIN ISO 12413 for conventional grinding wheels are allowed for operation. The inscription and coloured mark indicate the permissible maximum working speeds. This maximum speed v_s is considerably lower than the bursting speed v_{br} determined in the experiment depending on the safety factor S_{br}. Due to the square connection with the turning energy, the following relation applies:

$$S_{br} = \left(\frac{v_{br}}{v_s}\right)^2 \tag{13.13}$$

For machine-operated grinding with a closed working area (safe covering of the workspace) $S_{br} = 1.75$, without covering $S_{br} = 3$ has to be complied with. When a wheel is first introduced into a clamp (mostly clamping flanges), the following tests have to be carried out by the specialised staff:

- Visual test for tears, bursts or other damages.
- Ring test (only sensible for vitrified-bound wheels) for clear sound (ok) or rattling resp. dull sound (not ok).
- Clamping in special flanges.

- Test run in the machine with the maximum drive of the grinding spindle, maximum speed of the wheel, duration 1 min.

For the operation it is to be observed that porose grinding wheels are not allowed to be flooded by cutting liquid when stopped due to the risk of imbalance.

13.6 Grinding Processes

The grinding process can be described by input, process and output variables from a system-technical point of view (see also Sect. 1.3). The input variables are divided into system and manipulated or set variables (Fig. 13.18). The system variables are described by the workpiece (physical, chemical properties, original and machined part form and dimensions), the grinding wheel specification, the machine (type, static and dynamic properties), the dressing tool and the cooling lubricant system. The manipulated or set variables are cutting speed, depth of cut, feed and dressing result as well as the set pressure and the flow rate of the cooling lubricant. In contrast with the system variables, the manipulated variables can be adjusted to the process quickly. The evaluation of the grinding process occurs via process variables by means of the cutting forces, power, energies, temperatures, vibrations as well as the grinding time. Workpiece-specific variables such as form and dimension accuracy, surface quality as well as surface zone properties, which have considerable influence on the functional performance of the component, are used to describe the output variables. Further output variables are wear, micro-

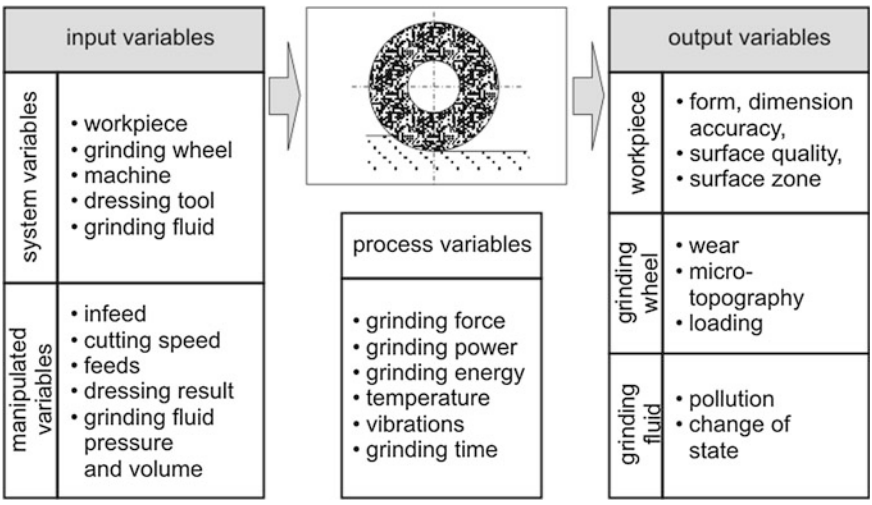

Fig. 13.18 Characteristics of the grinding process

topography and the loading-up of the grinding wheel as well as the pollution and alterations of the grinding fluid.

13.6.1 Input Variables

The productivity of the grinding process is described by the material removal rate Q_w (material flow rate, which is separated from the workpiece) [SAL91]. Figure 13.19 shows the variables required for the peripheral and side surface grinding to calculate the material removal rate. It follows at

$$Q_w = a_e \cdot a_p \cdot v_{ft} \tag{13.14}$$

from the working depth of cut a_e and the width of cut a_p, which add up to the engagement cross-section $A_w = a_e \cdot a_p$ and from the tangential feed speed v_{ft}, which stands normally to the cross-section. The depth of cut a_e is measured in the working plane (spanned between feed and cutting speed vector), the width of cut a_p is measured normally to the working plane. Figure 13.20 contains information on the material removal rates for other grinding processes than the peripheral and side surface grinding. Generally, the following applies to other surface grinding processes,

$$Q_w = A_w \cdot v_f, \tag{13.15}$$

where A_w[2] is the engagement cross-section normal to the main feed speed v_f.

The geometrical and kinematic engagement conditions are of relevance to the chip formation in the effective zone. The geometric contact length l_g is entered in Fig. 13.19. Together with the width of cut, the geometric contact surface $A_k = a_p \cdot l_g$ results from this. The geometric contact length can be determined from the grinding wheel radius r_s and the depth of cut a_e at

$$l_g = r_s \cdot \arccos\left(\frac{r_s - a_e}{r_s}\right) \tag{13.16}$$

or for $r_s \gg a_e$

$$l_g = \sqrt{2 \cdot r_s \cdot a_e} \tag{13.17}$$

For a determination of the contact length and the contact surface independently from the tool and workpiece measurements and, in addition, independently from the process, the equivalent (equivalent to surface grinding) radius r_{eq} resp. diameter d_{eq} is defined. The following applies

[2] Here A_w determines the engagement cross-section and is not to be confused with the removal surface rate.

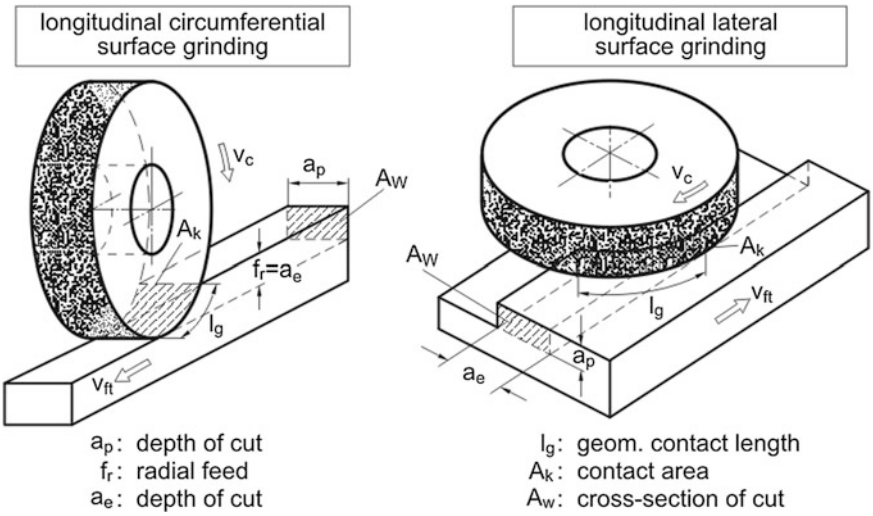

Fig. 13.19 Characteristics of the grinding process

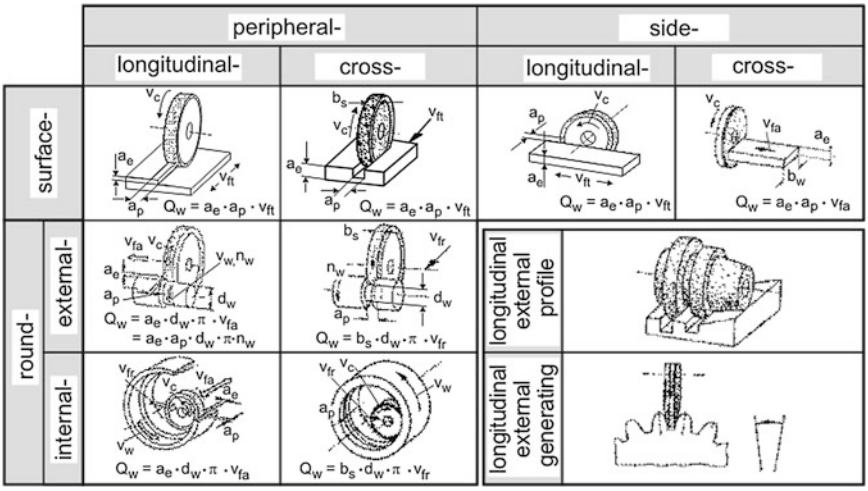

Fig. 13.20 Important grinding processes (according to DIN 8589)

$$r_{eq} = \frac{r_w \cdot r_s}{r_w \pm r_s}, \tag{13.18}$$

at which the addition in the denominator stands for external cylindrical grinding and the subtraction for internal cylindrical grinding. Figure 13.21 represents the concept figure for the identification of r_{eq} and shows a comparison for external and internal cylindrical grinding at different radius conditions.

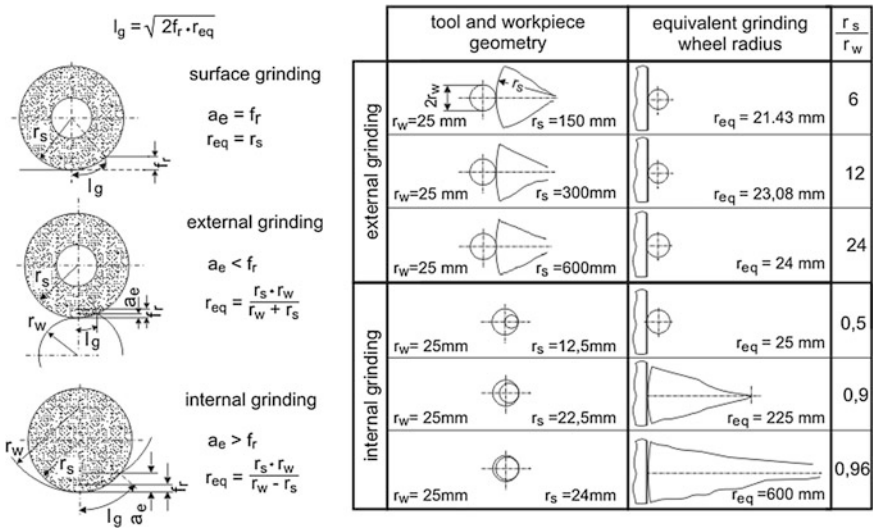

Fig. 13.21 Description of the equivalent radius

The geometric contact length is a calculation variable, which contains several simplifications as an approximation. It does not consider

- the entire kinematic of the effective partners, i.e., the cycloidic cutting path of the tool against the workpiece,
- the elastic deformation of the bodies involved as a consequence of the grinding forces,
- the fact that the surfaces of the grinding wheel and the workpiece, which are in contact, are not geometrically smooth but actually very rough and
- that the real contact surface only represents a fraction (in an order of 1 %) compared with the total surface of the workpiece engaged due to the contact of only single grains or cutting edges of the grinding wheels.

The kinematic contact length l_k considers the feed and cutting speed and assumes smooth effective partners. At a good approximation, it is

$$l_k = l_g\left(1 \pm \frac{1}{q}\right), \ (+: \text{ down grinding}, -: \text{ up grinding}) \tag{13.19}$$

at which the speed relation is $q = v_s/v_f$ (Fig. 13.22). At this, the addition stands for the up grinding, the subtraction for the down grinding. So in common grinding processes with $q = 60$, l_k and l_g differ from each other by 1.6 %. In creep feed grinding ($v_{ft} \ll v_c$), the difference is considerably lower. Noteworthy differences can only occur in speed stroke grinding, i.e., very high feed speed.

So far, it has not been considered that the actual contact between grinding wheel and workpiece only takes place via the active abrasive particles. So the real

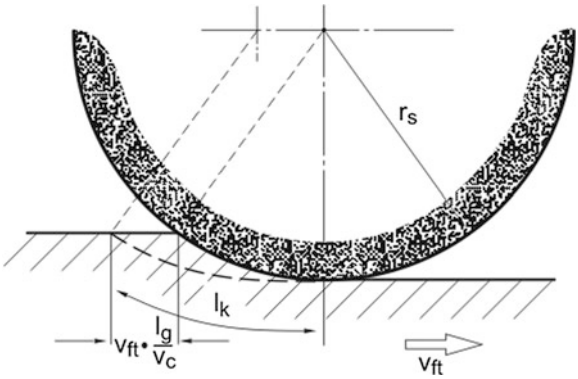

Fig. 13.22 Kinematic contact length

contact surface is far smaller than calculated so far. A rough estimation of the relation between the real and the so-far mathematically determined contact area A_e/A_c is possible by considering the yield strength of the material [ROW93]. If the average pressing under the abrasive particles tolerable until material flow is p_{max}, the following applies:

$$F_n = A_e \cdot p_{\max}, \tag{13.20}$$

and thus

$$\frac{A_e}{A_c} = \frac{F'_n}{p_{\max} \cdot l_c} \tag{13.21}$$

Tests show an order of $A_e/A_c < 0.01$.

Since the grinding width or the depth of cut is generally large compared with the occurrence at the single grain, it is assumable with sufficient approximation that the same chip formation conditions apply along the width of cut. Thus, the set and process variables are sensibly related to the width of cut, such as e.g., the related material removal rate

$$Q'_w = \frac{Q_w}{a_p} \tag{13.22}$$

Forces, energies or powers, such as wear volumes are purposefully divided by the width of cut so as to make them technologically comparable.

The material removal rate is established by externally determined variables. So Q_w is also called the external material removal rate Q_{wa}. This external material removal rate has to be identical with the volume, which is cut per time unit by the cutting motion—marked by the cutting speed v_c—and the engagement of the single cutting edges. The volume rate produced by the cutting motion is indicated as the internal material removal rate Q_{wi}. If, according to Kurrein [KUR27], one assumes that a "material band" of the thickness h_{eq} is separated from the workpiece with the cutting speed, the following results (Fig. 13.23).

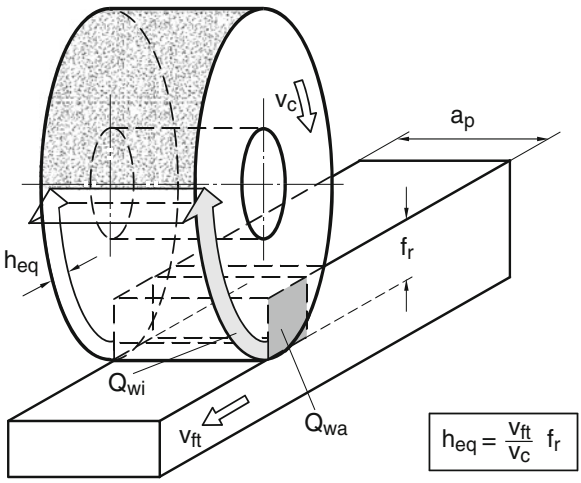

Fig. 13.23 Equivalent chip thickness h_{eq}

$$Q_{wi} = h_{eq} \cdot a_p \cdot v_c. \tag{13.23}$$

From the mentioned identity

$$Q_{wa} = Q_{wi} \tag{13.24}$$

the equivalent chip thickness results at

$$h_{eq} = f_r \cdot \frac{v_{ft}}{v_c} \tag{13.25}$$

or with the speed relation $q = v_c/v_{ft}$

$$h_{eq} = \frac{f_r}{q} \tag{13.26}$$

h_{eq} is a mathematical variable, which does not indicate the actual cutting thickness but a far smaller one, since a continuous band is not cut from the workpiece, only single grains or cutting edges are effective.

According to M. C. Shaw [REI56], the average chip thickness at the grain resp. the cutting edge h_c can be determined from the number of grains resp. cutting edges N_A per unit area of the active grinding surface. If N_A is detected by counting the grains in the top view of the grinding wheel, the following assumptions are made:

- every grain participates in the cutting,
- every grain lies at the same height in the external diameter,
- every grain separates the overlapping volume that it penetrates on the workpiece. Elastic deformations and plastic displacement (ploughing) or chipping of material does not occur,
- every grain has a free contact length without any cutting overlapping with grains moving before or after (no path overlappings) occurring.

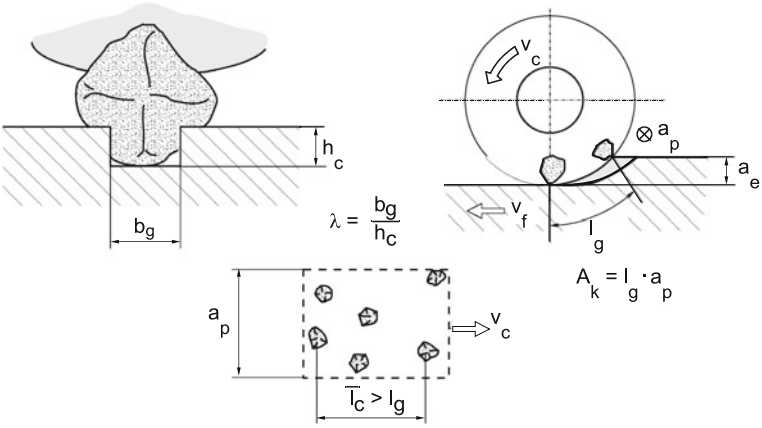

Fig. 13.24 Grain form and grain density

According to Fig. 13.24, the effective average cross-section of a grain is

$$A_g = b_g \cdot h_c \tag{13.27}$$

and with the form factor

$$\lambda = \frac{b_g}{h_c} \tag{13.28}$$

the total of the cross-section area A_c cut with the cutting speed is

$$A_c = \sum A_g = A_g \cdot N_A \cdot A_k = \lambda \cdot h_c^2 \cdot N_A \cdot a_p \cdot \left(2 \cdot f_r \cdot r_{eq}\right)^{1/2} \tag{13.29}$$

at which A_k is the contact area with $A_k = l_g \cdot a_p$. Consequentially, equalizing the internal and external material removal rate results in $Q_{wi} = Q_{wa}$:

$$A_c \cdot v_c = f_r \cdot a_p \cdot v_{ft} \tag{13.30}$$

the average chip thickness

$$h_c = \left(\frac{v_{ft}}{v_c} \cdot \frac{1}{N_A \cdot \lambda} \cdot \frac{f_r}{l_g}\right)^{1/2} \; with \, l_g = \sqrt{2 \cdot f_r \cdot r_{eq}} \tag{13.31}$$

Obviously, the assumption that all grains participate equally in the grinding process, i.e., with the same cross-section A_g, is actually not fulfilled; since the abrasive particles are generally arranged without rules within the bonding (except in a galvanic bonding). A further-going theory therefore considers the distribution of the grains perpendicular to the active grinding plane. Büttner and Triemel determined the grain distribution from the concentration of the grinding material in the volume of the grinding wheel [BÜT68, TRI76].

For the wheel volume V_s, the following applies

$$V_s = V_g + V_b + V_p \tag{13.32}$$

with the grinding material volume V_g, the bonding volume V_b and the pore space V_p. The composition is to be detected by an Archimedean weighting or from the manufacturer specification.

The number of grains per volume unit N_V can be defined as follows with the aid of the average volume of a grain V_{ge} or from the grain concentration C and the density of the grinding material ρ_g

$$N_V = \frac{V_g}{V_{ge} \cdot V_s} = \frac{C}{\rho_g \cdot V_{ge}} \tag{13.33}$$

The following applies for the volume of a grain with the shape factor q_e, which turns into $q_e = 1$ for the ball shape:

$$V_{ge} = q_e \frac{1}{6} \pi d_g^3 \tag{13.34}$$

According to Fig. 13.25, an imaginary area of size "1" in distance $z \geq d_g$ off the grinding wheel periphery is penetrated by a grain number N_{A0}. The following applies

$$d_g \cdot N_v \cdot ''1'' = N_{A0} \cdot ''1'' \tag{13.35}$$

$$N_{A0} = d_g \cdot N_v \tag{13.36}$$

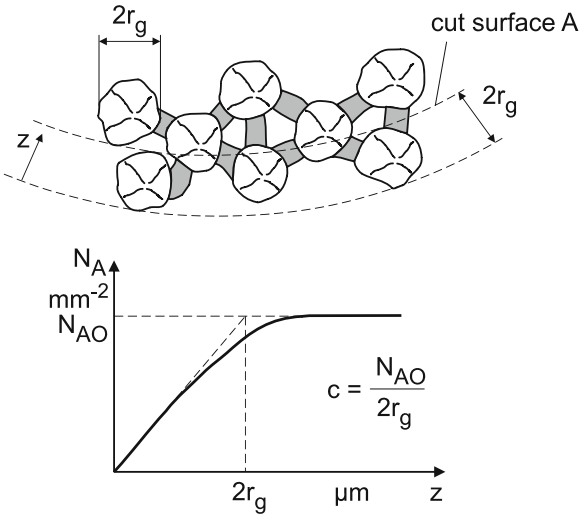

Fig. 13.25 Grain distribution and grain density

At this it is pre-assumed that the volume-related grain density N_v is constant, independently from z. This does not apply to $z < d_g$. In fact, the area-related grain number N_A increases linearly with z in this domain. In addition, the limit value N_{A0} is already reached at a low penetration depth z into the grinding layer due to influences of the free edge. Figure 13.25 illustrates the gradient of the grain number per area unit above z

$$c = \frac{dN_A}{dz} = \frac{N_{A0}}{2r_g} \tag{13.37}$$

$$c_0 = N_v \tag{13.38}$$

It was possible to determine the grain density by measurement with a thermoelectric method [KAI75]. According to this, we can actually assume a constant grain density c_o in the active cutting edge space (Fig. 13.26), which reaches down to a cutting edge space depth of $z \approx 0.3\ d_g$. The cutting edge space depth decreases with an increasing cutting edge density, i.e., higher grain concentration, finer grains and higher grain holding capacity of the bonding.

The determination of the grain density resp. grain number per area unit from the grinding material concentration presumes that every grain has only one cutting edge. Depending on the dressing process and the type of bonding and the grinding material, a grain can develop several cutting edges [WER71, LOR75]. But even in that case, it is possible to assume with sufficient approximation that the cutting edge density is constant, i.e., the number of cutting edges per area unit increases linearly with the penetration depth into the cutting edge space. The chip thickness h_c can then be determined with the grain resp. cutting edge distribution.

With this knowledge of the cutting edge resp. grain distribution over the penetration depth into the active grinding space, an extended chip thickness model can

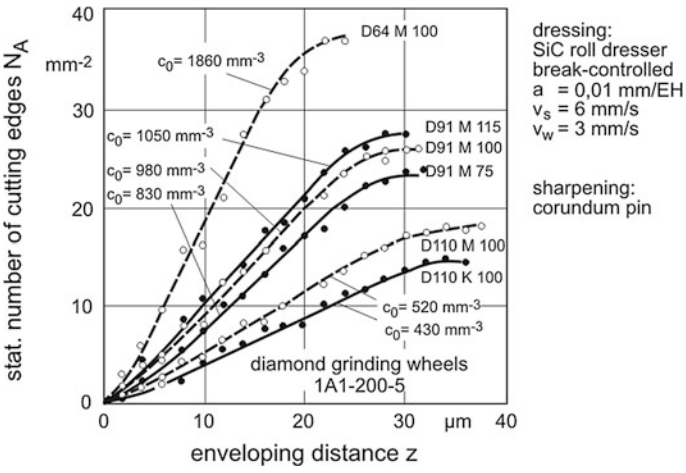

Fig. 13.26 Sum frequency of cutting edges in diamond grinding layers

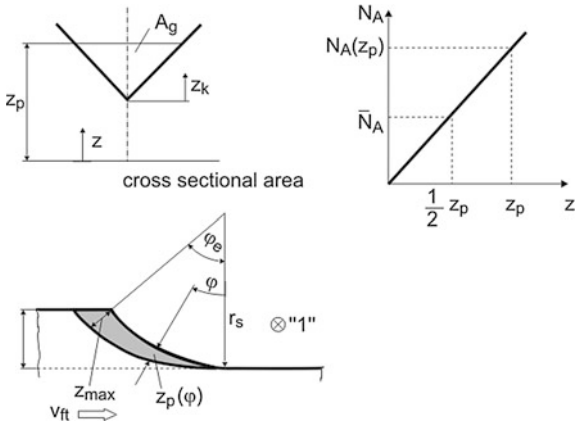

Fig. 13.27 Grain shape, grain distribution and kinematics for the chip thickness model

be developed, based on the considerations of Büttner [BÜT68], Triemel [TRI76], Kassens [KAS69] and Lortz [LOR75].

The internal material removal rate results from the number of grains currently engaged N and the average cutting cross-section per grain A_g

$$Q_{wi} = N \cdot A_g \cdot v_c \tag{13.39}$$

An average grain shape with an obtuse angled cross-section (triangle) is assumed for the average grain cross-section (Fig. 13.27),

$$A_g = c_1 \cdot z_K^2 \tag{13.40}$$

with c_1 describing this grain shape. In principle, a different function, e.g., an exponential function as in [WER71] could be determined for A_g. However, since the determination of the average grain shape is only possible with limited accuracy in any case, this bears no advantage. The number of engaged grains results from the grain distribution with

$$N_A = c_0 \cdot z_p \tag{13.41}$$

where z_p is the penetration depth of a grain into the material (Fig. 13.27). Due to the constant grain density above z, the average number of grains per area at any position φ of the engagement bend is

$$\overline{N}_A = \frac{1}{z_p} \cdot \int_0^{z_p} c_0 \cdot z \cdot dz = \frac{1}{2} c_0 \cdot z_p \tag{13.42}$$

dN grains are active above a bend increment of the length $r_s \cdot d\varphi$ and the width "1".

$$dN = \overline{N}_A \cdot \text{``1''} \cdot r_s \, d\varphi \tag{13.43}$$

Due to the constant grain density, the average grain cross-section at a point φ is

$$A_{g(\varphi)} = \frac{1}{z_p} \cdot \int_0^{z_p} c_1 \cdot (z_p - z)dz = \frac{1}{3} c_1 \cdot z_p^2 \tag{13.44}$$

Thus, over the entire engagement bend, the sum of the grain cross-sections is

$$\sum \mathrm{A_g} = \int_0^{\varphi_e} \mathrm{A_{g(\varphi)}\,dN} = \frac{1}{6} \mathrm{c_0 \cdot c_1 \cdot ``1'' \cdot} r_s \cdot \int_0^{\varphi_e} \mathrm{z_p^3\,d}\varphi \tag{13.45}$$

For the kinematics of the peripheral grinding, the following applies

$$\frac{\varphi}{\varphi_e} = \frac{\mathrm{z_p}}{\mathrm{z_{max}}} \tag{13.46}$$

and with

$$\varphi_e \approx 2 \cdot \left(\frac{\mathrm{f_r}}{2r_s}\right)^{1/2} \tag{13.47}$$

the sum of the grain cross-sections over the entire engagement bend is then $\mathrm{r_s} \cdot \varphi_\mathrm{e}$

$$\sum \mathrm{A_g} = \frac{1}{12} \cdot \mathrm{c_0 \cdot c_1 \cdot ``1'' \cdot r_s \cdot z_{max}^3} \left(\frac{\mathrm{f_r}}{\mathrm{d_s}}\right)^{1/2} \tag{13.48}$$

From $\mathrm{Q_{wi}} = \mathrm{Q_{wa}}$ results

$$\mathrm{f_r \cdot ``1'' \cdot v_{ft}} = \sum \mathrm{A_g \cdot v_c} \tag{13.49}$$

and thus finally the maximum grain penetration depth (cutting depth)

$$\mathrm{z_{max}} = \left(24 \cdot \frac{v_{ft}}{v_c} \cdot \frac{1}{c_0 \cdot c_1}\right)^{1/3} \cdot \left(\frac{\mathrm{f_r}}{\mathrm{d_s}}\right)^{1/6} = \left(24 \cdot \frac{1}{\mathrm{c_0 \cdot c_1}} \cdot \frac{\mathrm{Q'_W}}{\mathrm{v_c \cdot 1_g}}\right)^{1/3} \tag{13.50}$$

A simplified illustration of the correlations between the grain penetration depth and the manipulated variables of the grinding process illustrate the possibilities of influence on the cutting depth in the grinding process

$$z_{max} \approx \frac{1}{\mathrm{d_g}} \left(\frac{\mathrm{Q'_w}}{\mathrm{c_1 \cdot v_c \cdot 1_g}}\right)^{1/3} \tag{13.51}$$

Further models on grinding forces, roughnesses and grinding energies can be established on the basis of this chip thickness model [WOB91, TÖN92, PAU94, FRI02].

13.6.2 Process Variables

The mechanical energy applied during the grinding process is almost totally transformed into thermal energy. This amount of heat can evoke geometrical deviations on the workpiece, alter its surface zone and accelerate the tool wear. Thus, the contact zone temperature represents an important process variable. It is, however, difficult to measure due to the rapid temperature changes and the resulting steep temperature gradients. In addition, the contact zone is not readily accessible and mostly surrounded by cutting liquid. In principle, the temperature measuring process can be differentiated into heat conduction and heat radiation. The most common methods are illustrated in Fig. 13.28 [KAR01].

Due to the necessity to measure as closely as possible to the contact point, the workpiece or the grinding wheel has to be prepared for all methods, which use heat conduction, and for the pyrometer measuring process. Therefore, the listed measuring methods are only applied in research. A direct temperature measuring method applicable in practise for process supervision does not exist until now. It is possible, however, to indirectly draw conclusions concerning the surface zone influence in the workpiece as described in Chap. 15. The temperatures mentioned in Fig. 13.29 are recorded during external plunge grinding with a minimum quantity lubrication (MQL) and without any kind of cutting lubrication with a thermographic system at a distance of 30 mm from the contact zone. The tests include different combinations of cutting and feed speed and material removal rates during the grinding process of ball bearing steel 100Cr6 with micro-crystalline Al_2O_3 and CBN grinding wheels.

In Fig. 13.29, the X-ray-measured workpiece residual stresses are set at the measured temperatures ϑ_M. The result is a uniform transfer function for different

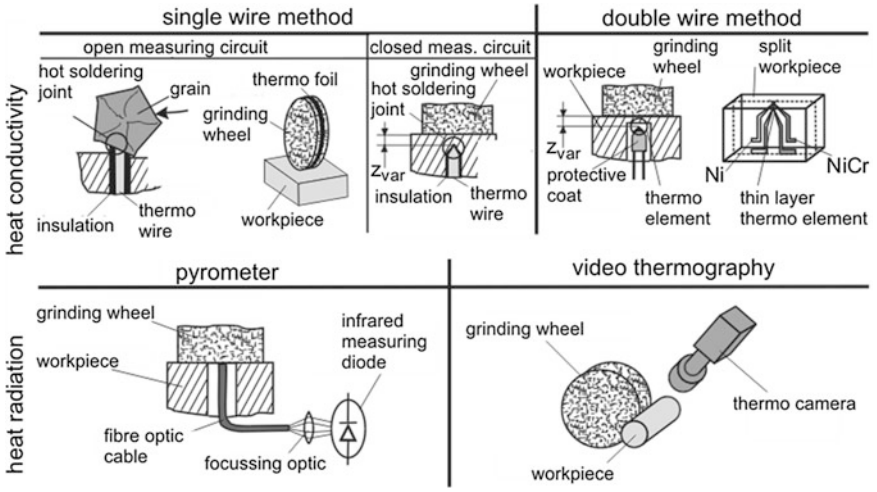

Fig. 13.28 Temperature measuring methods for geometrically-undetermined cutting (according to Karpuschewski)

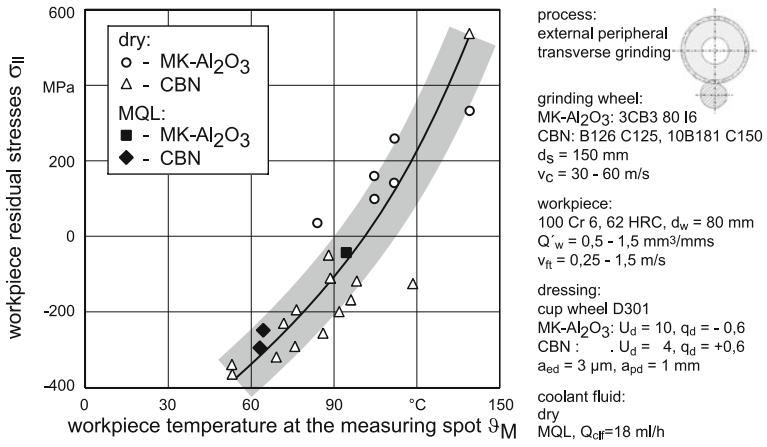

Fig. 13.29 Workpiece residual stresses depending on the workpiece temperature

tools and engagement conditions. Workpiece residual stresses between −400 and 500 MPa can be assigned to the temperatures. An increase of the temperatures and thus of the residual stresses can be detected at an increase of the material removal rate with any kind of grinding material. An increase of the measured temperatures is detectable at an increasing cutting speed and using the micro-crystalline Al_2O_3 grinding wheel. In CBN grinding, the variation of the cutting speed does not influence the temperature. A decrease of the workpiece temperature can be reached by increasing the workpiece speed (tangential feed speed). The differences between the two grain types can be explained with the different properties. CBN grains have a high wear resistance and heat conduction. Accordingly, the heat amount, which arrives inside the workpiece is lower, which results in lower workpiece temperatures [BRU98].

The mechanical power P_c is fed into the grinding process.

$$P_c = F_t \cdot (v_c \pm v_{ft}) \; (+ : \text{ up grinding} - : \text{ down grinding}) \tag{13.52}$$

Since $v_c \gg v_{ft}$ generally applies, the following can be concluded:

$$P_c = F_t \cdot v_c \tag{13.53}$$

Apart from a negligible rest of $(1 - k_1) < 0.03$, which is transformed into dislocation energies and lattice distortion, i.e., residual stresses, this power is transformed into heat. The heat flow is $L = k_1 P_c$. This heat flow drains off via the tool L_s, the workpiece L_w, the chips L_{ch}, the cutting fluid L_1 and the environment L_r. The main proportion is absorbed by tool and workpiece [CHO86].

$$L_s + L_w = k_2 \cdot L, \tag{13.54}$$

$$k_2 \approx 0.8 \div 0.9 \tag{13.55}$$

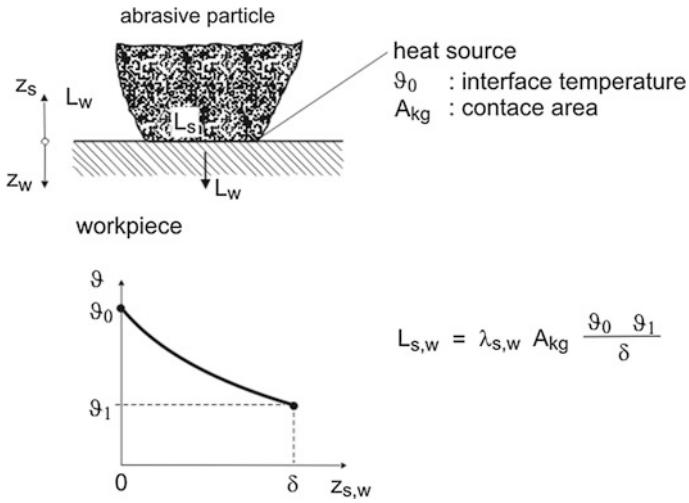

Fig. 13.30 Energy balance on the abrasive particle

A simplified consideration of both parts is useful to explain the different thermal surface zone influences in the case of conventional grinding materials and boron nitride (Fig. 13.30). At this, a unidimensional, stationary heat conduction is pre-supposed and that the same temperature ϑ_1 prevails in the media involved at a distance $\delta_s = \delta_w = \delta$ from the contact plane. Then the following applies:

$$L_{s,w} = \lambda_{s,w} \cdot A_{kg} \frac{\vartheta_0 - \vartheta_1}{\delta} \tag{13.56}$$

with the heat conduction co-efficients $\lambda_{s,w}$. The following results from $k_2 \cdot L = L_s + L_w$:

$$L_s = \frac{k_2 L}{1 + \lambda_w / \lambda_s} \tag{13.57}$$

$$L_w = \frac{k_2 L}{1 + \lambda_s / \lambda_w} \tag{13.58}$$

For grinding materials with different heat conductions, such as corundum with λ_{sk} and boron nitride with λ_{sb}, the following results for the heat flows L_{Wk}, L_{Wb}

$$\frac{L_{wk}}{L_{wb}} = \frac{\lambda_w + \lambda_{sb}}{\lambda_w + \lambda_{sk}} \tag{13.59}$$

For the media steel ($\lambda_w = 50$ W/mK), corundum ($\lambda_{sk} = 29$ W/mK) and boron nitride ($\lambda_{sb} = 1{,}300$ W/mK) follows

$$\frac{L_{wk}}{L_{wb}} = 17 \tag{13.60}$$

This means that when grinding with corundum, the 17-times heat amount flows into the workpiece compared with boron nitride. The grinding wheel based on boron nitride quasi acts as a scoop wheel for the heat energy due to the good heat conduction.

13.6.3 Output Variables

Grinding wheels wear. Grain and bonding wear occurs. The following types of wear can be differentiated for grain wear:

Pressure softening: This phenomenon can occur with corundum, which does have a melting point of 2,050 °C, but whose strength already drops to a sixth of its compression strength at 1,200 °C compared with room temperature [STA62]. As a consequence of the pressure softening, high friction forces and rounded cutting edges occur, which additionally increases the chip formation temperatures. An unstable condition may be the consequence, which leads to a failure of the grinding wheel. The volume or radius wear is low.

Abrasion: As a consequence of the friction between grain and workpiece, mechanical abrasion occurs (Fig. 13.31). The grain is continuously removed and also produces undesired, because friction and shear force increasing, rounded cutting edge in this case. The volume or radius wear is low.

Splintering: Due to the thermal load and following rapid cool-off, but also due to mechanical load at a sufficient splintering capacity of the abrasive particle, parts

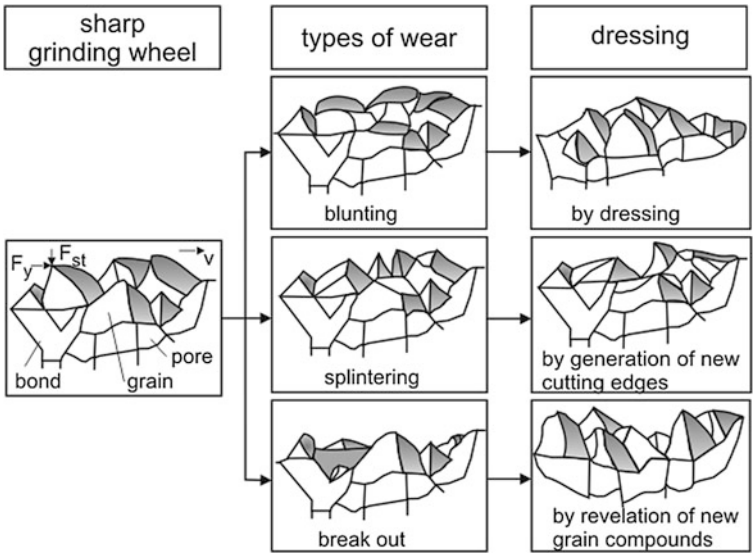

Fig. 13.31 Types of wear and sharpening in the grinding process

of the grains splinter and thus produce new cutting edges. This type of wear is therefore favourable, since the volume and radius wear is actually higher compared with the pressure softening and the abrasive wear, but still sufficiently low and sharp cutting edges develop nevertheless. The capacity of splintering can be marked with the friability test (see Sect. 13.2).

Breaking out: In this type of wear entire grains break out of the compound. The holding force of the bond is not enough, the bond is too soft. Strong volume and radius wear occurs. The grinding wheels do, however, maintain their grindability.

The wear of a grinding wheel is recorded numerically by the volume wear V_s or the radius wear Δr_s. The volume wear is directly included in the grinding ratio or the performance factor.

$$G = \frac{V_w}{V_s} = \frac{Q_w}{Q_s} \tag{13.61}$$

The G-ratio is dependent on the material of the workpiece, the grinding tool, the engagement variables, the conditioning and the grinding fluid among others. It therefore deviates within wide limits. When grinding with corundum on hardened steel 100Cr6 under average conditions and emulsion as grinding fluid, a G-ratio of 80 can be expected. When using CBN and under mineral oil, the G-ratio can be increased to 3,000 and more [GRA87].

In dimension and form precision grinding, the radius wear is mostly more considerable. That is the local abrasion of the grinding wheel after a certain grinding task or grinding time. The average radius wear speed is correlated with the grinding ratio, which results from a volume balance:

$$\frac{\Delta r_s}{\Delta t} = \frac{1}{G} \frac{f_r \cdot v_{ft}}{2\pi\, r_s} \tag{13.62}$$

Fine machining processes such as grinding generally produce surfaces for their final and usage condition. As explained in Chap. 16 about surface properties, the function properties of components, are fundamentally determined by geometrical and physical properties of their surfaces. Here, it is the question whether and how these properties can be achieved by means of the grinding process and its input variables.

The micro-geometrical surface formation can be described by different parameters such as the roughness parameters R_z and R_a, the bearing contact area ratio and others (see Chap. 16), depending on which function of the surface is essential. Often, the average roughness R_z is specified. In Fig. 13.32, the influences of some input parameters on the surface quality are stated concerning quality. Basically, the surface produced by grinding is connected with the micro-topography of the grinding wheel and the kinematic conditions, which the cutting edges are moved at on the workpiece. A first approximation as a dimension for the surface formation is the cutting thickness resp. the penetration depth of the cutting edges, as modelled in Sect. 13.7.1.

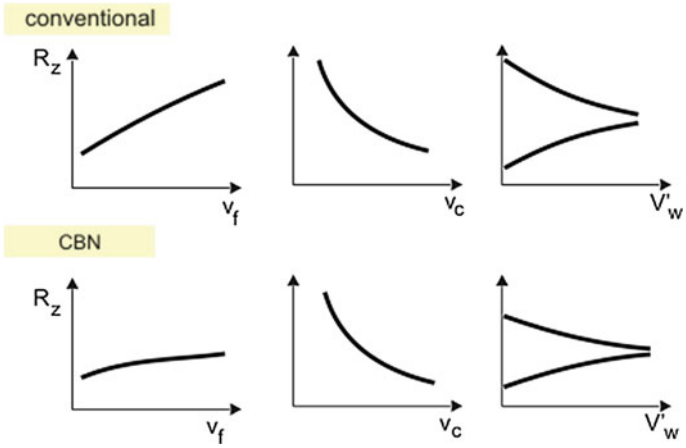

Fig. 13.32 Influence of the adjustment variables on the workpiece roughness

With regard to the wear behaviour Fig. 13.32 differentiates between conventional and super hard grinding materials, at which the same trends can be determined for both, although with CBN, the alterations of the roughness parameters are considerable stretched time-wise [HEU92]. The schematic illustrations show that the roughness increases with increasing feed speed, which can be ascribed to the increase in cutting thickness. For the influence of the cutting speed the corresponding is valid: when it is increased, the cutting thickness decreases. The grinding time resp. the cutting volume V'_w has an ambivalent effect according to the original microtopography of the grinding wheel, as Weinert demonstrated [WEI76] (see also Sect. 13.7.2). With a rough wheel, a smoothing effect shows after an originally higher roughness. Vice versa, with a very smooth wheel, a roughing and thus an increase of the roughness occurs on the workpiece due to wear effects.

Apart from this kinematic approach, the material behaviour is to be considered, namely whether the material tends towards ductile or brittle deformation and separating behaviour under the given process conditions (cutting thickness, temperature distribution). Investigations on one-grain-scratching brittle-hard materials have demonstrated that below a certain scratching normal force, any number of long, tear-free, plastically deformed scratching traces show on the component. At higher scratching normal forces resp. cutting thicknesses, directly after the scratching process load relief tears break open in the area behind the cutting edge due to residual tensile stresses and increasingly lead to brittle material separation (Fig. 13.33). In principle, these conclusions can be transferred to the grinding process, where a large number of abrasive particles is engaged [ROT94]. At this, the size of the average single grain cutting thickness has a decisive influence on the occurring material separation. Lower single grain cutting thicknesses—e.g., produced by using fine-grained grinding wheels—cause a rather ductile material separation, whereas the use of coarse-grained grinding wheels increasingly leads to brittle material separation [LIE98].

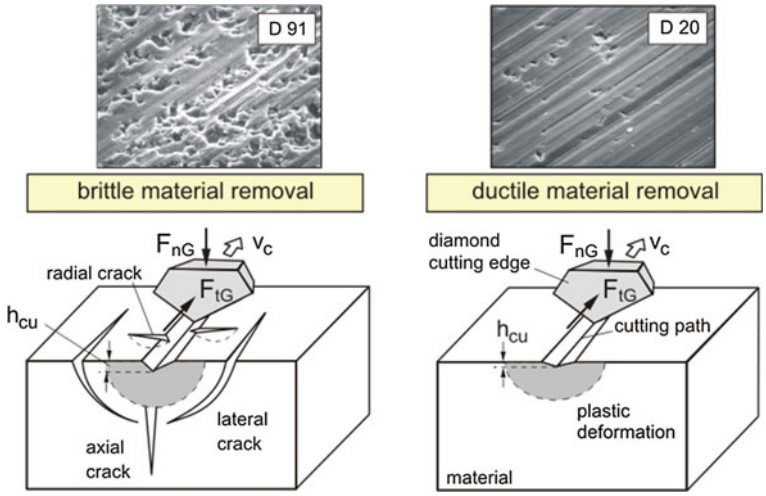

Fig. 13.33 Material separation mechanisms on brittle-hard materials (according to Lawn and Marshall)

The quality of ground components not only depends on the compliance with dimension and form tolerances and a required surface quality, but also on the physical properties of the workpiece surface zone. The physical surface zone properties are determined as the structure condition and the residual stresses in the surface near layers of the machined workpiece [BRI82]. Hardness alterations can also provide information about the structure of the surface zones. High thermal influences can lead to the loss of hardness or—under extreme conditions—even to new hardening zones with underlying soft skin. Such structure alterations significantly deteriorate the usage properties of the components, in addition, steep hardness gradients in connection with surface residual stresses can cause cracks in the component [BRI91] (see Chap. 16).

The superposition of thermal and mechanical effects on the development of residual stresses is explained by *Brinksmeier* by applying residual stresses above the contact area-related grinding power P_c'' [BRI91]. The power results from the product of the relative speed between workpiece and grinding wheel and the tangential force F_t. It is referred to the contact surface formed by the engagement width a_p and geometrical contact length l_g.

$$P_c'' = \frac{F_t \cdot (v_s \pm v_{ft})}{a_p \cdot l_g} \left(W/mm^2\right) + \text{down grinding} - \text{up grinding} \tag{13.63}$$

If the workpiece speed is considerably lower that the grinding wheel speed, the obtained grinding power can be calculated with a good approximation as follows:

$$P_c'' = \frac{F_t \cdot v_c}{a_p \cdot l_g} \left(W/mm^2\right) \tag{13.64}$$

At very low grinding power, at first only thermally-conditioned residual stresses by means of external friction are to be expected. Plastic deformations caused by mechanical load lead to the development of residual compressive stresses. The temperatures, which rise with increasing grinding power, reduce the residual compressive stresses maximally induced by mechanical effect and, at the same time, lead to a continuously growing dominance of the terminally-conditioned residual tensile stresses. The thermal and mechanical influences overlap in a highly non-linear way so that a simple superposition is inadmissible and the illustration can only by schematic. A lower thermal load of the component leads to a more favourable course of the resulting residual stresses. This effect can be obtained by exchanging the grinding material or cutting liquid or by reducing the cutting speed or the material removal rate [BRI91].

Heuer [HEU92] demonstrates the limits of this model notion. An increase of the tangential feed speed at a constant cutting speed can lead to higher contact surface related grinding powers at a parallel lower residual stress level. *Karpuschewski* therefore considers the heat penetration time and defines a path energy (energy per unit path) as the effect referring to a cutting volume unit and describes the resulting residual stress condition as follows (k: transfer coefficient) [KAR95]:

$$\sigma_{||} = k \cdot \frac{e_c \cdot a_e}{l_e} (MPA) \tag{13.65}$$

Another approach for the description of the energies converted in the grinding process and their effects on the residual stresses remaining within the component is proposed by *Lierse* [LIE98]. He applies observations from the welding and laser technology, at which the contact time on the surface is directly considered for the calculation of a contact area-related energy and uses the parameter

$$E_c'' = P_c'' \cdot t_k = P_c'' \cdot \frac{l_g}{v_{ft}} = \frac{F_t \cdot v_c}{a_p \cdot v_{ft}} \left(J/mm^2\right) \tag{13.66}$$

during his investigations on mechanic and thermal effects in grinding of technical ceramics.

The thermal workpiece damage in grinding machining is influenced by the settings of the adjustment and system variables. Not only the primary process variables influence the thermo-physical processes while grinding. Also variables, which influence the grinding wheel topography decisively and thus also the described elementary processes during cutting, act on the development of thermal damages [BRI91]. This is also detectable for the used cutting fluids and their adjustment variables [GRA87, HEU92].

Basically it can be determined that any change in the contact zone between grinding wheel and workpiece affects the developing surface zone influence. Each one of these factors influences either the heat produced by cutting or the occurring forces resp. the heat distribution and thus causes a different influence, which can be determined by the developing residual stresses [BRI91]. For the layout of a

grinding process, it is necessary to avoid residual tensile stresses so as not to influence the functional behaviour of the components negatively (see Chap. 14).

In the following, the influence of important adjustment variables of the grinding process on the residual stress development in the machined workpiece will be described. At this, exclusively residual stresses parallel to the grinding direction will be consulted, since these mostly show bigger amounts in the direction of residual tensile stresses and are therefore considered more critical for the component behaviour [HAU80]. In Fig. 13.34, the residual stresses at the workpiece surface are illustrated for different related material removal rates via the cutting speed and the residual stress depth curves for different speed ratios. In the case of both large related material removal rates illustrated, an increase in the cutting speed leads to a drop of the measured residual stresses. For the low set material removal rate, residual compressive stresses exist for all conditions. The formerly discussed reduction of the cutting thickness and thus of the grinding forces at an increase of the cutting speed leads to a reduction of the residual stresses remaining on the workpiece surface for high related material removal rates. Although the cutting power necessary for cutting increases together with the increase of the cutting speed, the higher thermal power apparently does not have an effect on the residual stresses in the considered area.

The thermal and mechanical influence on the component material due to the grinding is not only limited to the immediate surface. According to the type and extent of the load, it has a varying depth effect [TÖN65]. For the evaluation of a grinding process, an analysis of this effect is of special interest, since higher residual stresses might exist below the surface, which means a strong damage of the component. For the interpretation of grinding processes it is necessary to

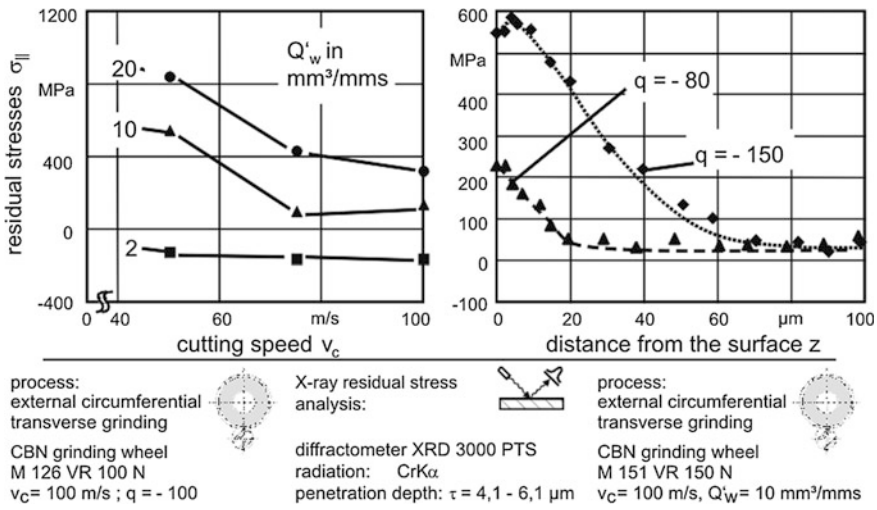

Fig. 13.34 Influence of the cutting and workpiece speed on the workpiece residual stresses of hardened components

possess knowledge of the depth effect of the adjustment variables. The influence of different speed conditions at a constant material removal rate can be gathered from the right part of Fig. 13.34. A higher speed ratio is achieved by reducing the workpiece rpm at the same cutting speed. As a consequence, the residence time of the heat produced by cutting is shorter than in the case of low speed conditions. The effect is clearly visible in the picture. The longer heat effective time leads to higher residual compressive stresses with a higher depth effect in the workpiece [CZE99].

The residual stress depth courses of different related material removal rates are illustrated in Fig. 13.35. At a low material removal rate of $Q'_w = 2$ mm^3/mms, residual compressive stresses occur at the surface. The depth effects of these mainly mechanically-conditioned residual stresses are but very low and amount to approx. 15 µm. The stress course shows a high gradient until the surface zone influenced by the compressive stress and then adopts the residual stress parameters of the basic compound. The hardness depth course and the grinding pattern of this sample also correspond to that of the undamaged basic compound.

At an increase of the related material removal rates to $Q'_w = 10$ mm^3/mms, the influence of the thermal load prevails compared with the mechanical load component. Only residual tensile stresses in the material are measured. The residual stress course drops from about 200 MPa residual tensile stresses at the surface about linearly to the condition of the basic compounds. The higher temperature introduced into the workpiece at this material removal rate leads to residual tensile stresses at the workpiece surface with a depth effect of 20 µm. In the micrograph, some annealing texture is recognisable at the workpiece edge and the measured hardness variables in the edge zone are lower than that of the undamaged original texture.

By means of an additional increase of the heat generated in the grinding process by a material removal rate of $Q'_w = 20$ mm^3/mms, the heat effective depths and the maximum values of the residual tensile stresses increase considerably.

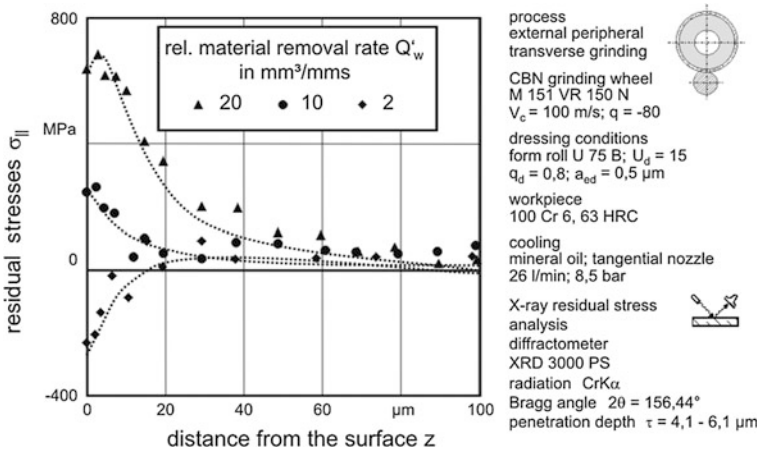

Fig. 13.35 Influence of the related material removal rate on the workpiece residual stresses

The radial spreading of the annealing texture rises analogically to the heat development. Due to the temperature effect, an annealing of the hardened texture occurs, which loses hardness because of the temperature-conditioned texture transformation. The temperature produced by the grinding process reaches values, which lead to the development of rehardening zones. An increase in hardness due to the rehardening is not detectable in the hardness course, since this zone is limited to few μm of depth. A measurement of the material hardness in this small area is not feasible.

13.7 Conditioning of Grinding Tools

13.7.1 Basics

Wear by splintering or break out of particles or wear caused by bonding erosion leads to the resharpening of grinding tools. This effect may be desired for rough grinding so as to avoid a conditioning of the tool. However, in finishing and fine grinding, conditioning is generally indispensable (E. Saljé: "If you cannot condition, you might as well not even start grinding".). The conditioning can serve three purposes (Fig. 13.36) [SPU89].

Profiling: This is about the restoration or new generation of a grinding wheel contour. If the cylindricity or the concentricity get lost or waves develop on the active grinding surface due to the wear of a grinding wheel, profiling becomes necessary, i.e., in this case a cylindric surface is generated. By profiling, even non-cylindric tool shapes can be generated for profile grinding. Profiling acts macro-geometrically.

Sharpening: If grinding tools are no longer suitable for grinding due to rounded cutting edges or loading (clogging of the chip spaces), sharpening can generate a new layer of particles or cutting edges. Sharpening acts micro-geometrically.

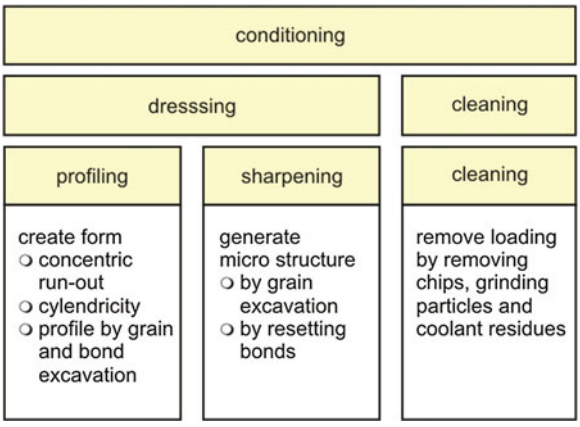

Fig. 13.36 Conditioning of grinding wheels (according to G. Spur)

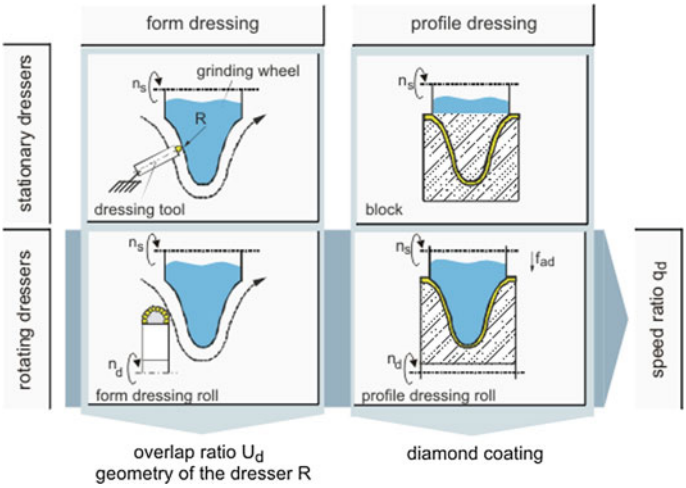

Fig. 13.37 Dressing process (according to Dr. Kaiser GmbH, Celle)

Cleaning: Cleaning removes residue consisting of workpiece and tool material or cutting liquid deposits. Cleaning does not alter the topography of the grinding tool; neither the particles nor the bonding are removed.

Profiling and sharpening together are also called dressing. Since in finishing or fine grinding the chip formation all the resulting effective parameters depend decisively on the dressing, i.e., the type and the adjustment parameters of this process, a grinding process can never be regarded by itself but must always be seen as a combination of conditioning/dressing and grinding.

Figure 13.37 illustrates dressing processes, which are distinguishable according to their kinematic resp. form generation [KAI09].

Grinding wheels can be dressed with rotatory and non-rotatory, fixed tools (Fig. 13.37). A second aspect of order is the type of shape generation. We distinguish form dressing, i.e., the controlled operation of the dressing tool, and profile dressing, at which the dressing tool receives the contour of the profile by copying.

Dressing tools can be handled with one or several cutting edges (consisting of one or several particles) (Fig. 13.38). The illustration shows the typical application of the Diaform process, at which the profile of the grinding wheel is generated by the controlled dressing of single diamonds.

The cutting elements consist of artificial or natural diamonds and are cased in a metal matrix. These diamonds can be coarse, form-cut or exist in another geometrically defined condition. They can be arranged in a stochastic distribution or according to a defined pattern on cylinder-, board- or slice-shaped carriers.

Form rolls are rotating dressers studded with diamonds at the circumference (Fig. 13.39). They are bi- or triaxially controlled so as to generate the wheel profile. Due to their multi-studding with diamonds, their durability is considerably higher than that of a single diamond. An additional advantage is that they are

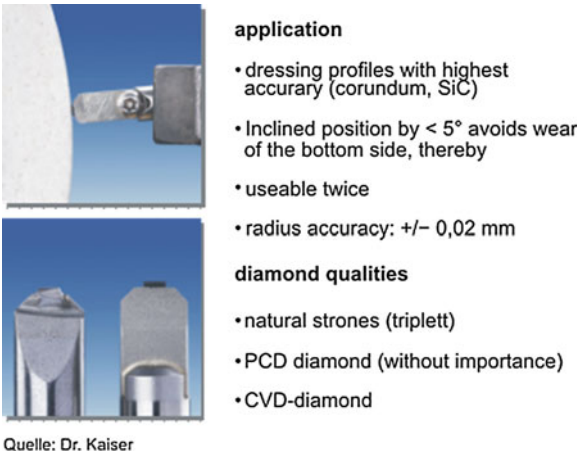

Fig. 13.38 Single particle dressers (works photo Dr. Kaiser GmbH, Celle)

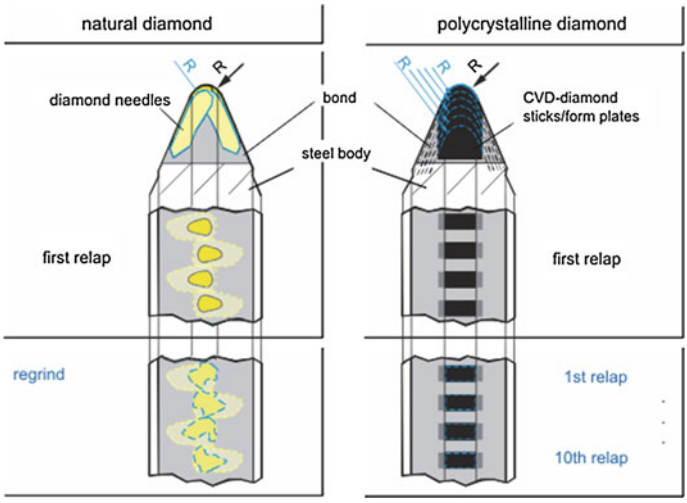

Fig. 13.39 Form rolls with set natural and poly-crystalline diamonds (works photo Dr. Kaiser GmbH, Celle)

largely independent from the profile to be generated. Therefore, they are suitable for small and medium-sized series. For large series, rotating profile tools, diamond profile rolls are used (Fig. 13.40). They bear the contour of the wheel profile. Due to the mostly necessary high-precision machining of such profile rolls and because of the entirely circumferential diamondization they are expensive, but do have a high durability and permit short dressing times, since only a short radial infeed is required.

Fig. 13.40 Profile roll with workpiece (works photo Dr. Kaiser GmbH, Celle)

Further differentiating factors for dressing tools are the deployed bonding systems (electro-plating or sintering bonds), the possibilities of diamondization (stochastic distribution by spreading, regular distribution by hand setting and one- or multi-layer tools) and the number of diamonds on the dresser in carat per cubic millimeter determined by the coating density. The properties of dressing tools, the influences of the adjustment parameters during dressing and practical deployment recommendations are clearly compiled by Minke [MIN99].

Basically, dressing corresponds to turning (Fig. 13.41). With the dressing feed f_{ad} and the intervention width a_{pd}, an overlapping ratio U_d can be defined as

$$U_d = \frac{a_{pd}}{f_{ad}} \tag{13.67}$$

The engagement width follows from

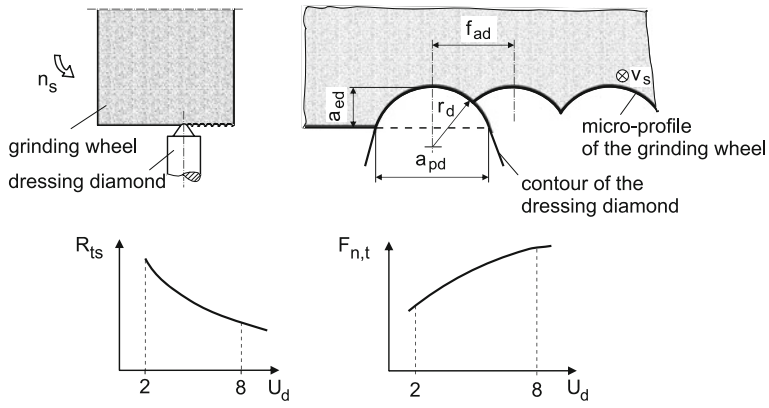

Fig. 13.41 Dressing with single diamonds

$$a_{pd} = 2 \cdot \left(2 \cdot r_d \cdot a_{ed} - a_{ed}^2\right)^{1/2} \tag{13.68}$$

and the dressing feed with the grinding wheel rotary frequency n_s at

$$f_{ad} = \frac{v_{fad}}{n_s}. \tag{13.69}$$

Common settings when dressing vitrified bonded grinding wheels are [MAG08]:

$$f_{ad} \leq 0.2\,\text{mm}, a_{ed} = 10\,\mu\text{m} \div 30\,\mu\text{m} \tag{13.70}$$

The effective parameters can be influenced in large areas with the degree of overlapping (overlap ratio) (Fig. 13.38), since the effective roughness of the active grinding surface and thus the number of active cutting edges of the grinding tool are strongly altered. The effective roughness R_{ts} is used to describe the cutting edge space topography of a grinding wheel. To determine this parameter, a test workpiece with fixed parameters is machined with the grinding wheel. The maximum roughness measured on the test workpiece produce the effective roughness of the grinding wheel [SCH68]. The effective roughness R_{ts} of the grinding wheel is

$$R_{ts} = \frac{f_{ad}^2}{8 \cdot r_d} \tag{13.71}$$

A higher degree of overlapping generates more active cutting edges with lower roughnesses on the workpiece. The forces and required power rise.

13.7.2 Conditioning of Conventional Grinding

Conventional grinding tools can generally be profiled and sharpened at the same time by the dressing tools shown in Fig. 13.37. The influence of the set conditions continuously gets lost with increasing grinding duration. The active cutting space of the grinding wheel changes due the occurring wear. The connected effects on the effective roughness of the grinding wheel at differently related material removal rates and dressing conditions for a fixed dresser are illustrated in Fig. 13.42. Depending on the initial effective roughness $R_{t,s0}$ of the grinding wheel caused by the dressing, with increasing grinding time, the grinding wheel tends towards a stationary roughness, which is independent from the dressing conditions. The upper part of the picture shows that at a constant roughness of the grinding wheel, with deployment time, different final roughnesses develop due to a wear-conditioned alteration of the cutting area. Vice versa, the lower part of the picture shows that, with deployment time, the initial roughness is altered and tends towards a stationary value. The cutting area of the grinding wheel quasi loses its memory [WEI76]. For the practical use in serial production it is of interest that a

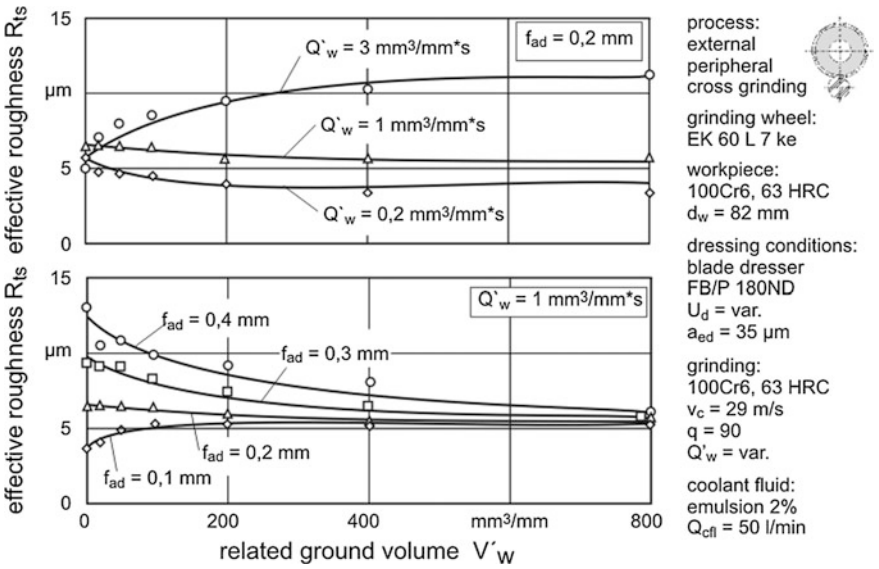

Fig. 13.42 Effective roughness depending on the related cutting volume for different adjustment parameters (according to K. Weinert)

steady grinding result can be obtained by means of the dressing strategy by hitting the stationary roughness already when dressing. On the other hand, very different roughnesses can be achieved in small batch production with the same wheel (grit size) due to the dressing [VER79].

The dressing of conventional grinding wheels with rotating tools is frequently used to condition profile wheels. At this, it is possible to work with a diamond studded dressing wheel analogue to the dressing with a single-grain diamond, at which the wheel has to be path-controlled in at least two axis or the profile to be generated contained in a diamond profile roll. The latter process is generally deployed in large serial production due to the high costs for the profile roll. Figure 13.43 illustrates the dependence of the initial effective roughnesses $R_{t,s0}$ of the grinding wheel profile achievable when dressing with profile rolls depending on the two parameters dressing speed ratio and radial dressing feed per rotation of the grinding wheel.

During the dressing process, the diamonds of the roll move in relation to the grinding wheel on cycloidic paths. At this, the shape of the curves depends on the speed ratio. If the diamond grains penetrate more steeply into the grinding wheel, the roughness of the grinding wheel increases. In same direction ($q_d > 0$), strongly bent paths develop in the area of the contact point, whereas the paths are elongated in the counter direction ($q_d < 0$). Analogue to these bends, greater effective roughnesses appear in the counter direction than in the same direction [SCH68]. With rising parameters for the radial dressing feed, the initial effective roughness also increases, whereas the roughness course maintains its basic tendency above

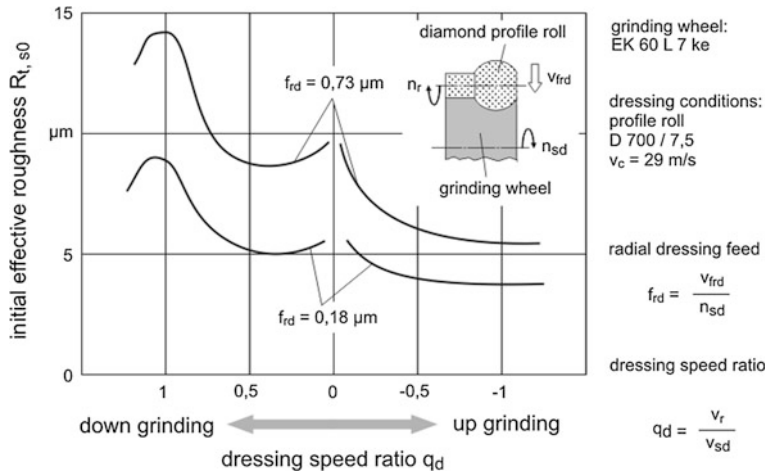

Fig. 13.43 Influence of the dressing conditions on the initial effective roughness in case of diamond profile rolls (according to Schmitt)

the feed speed ratio. In the case of the dressing speed ratio $q_d = 1$, a rolling-off (crushing) takes place between the grinding wheel and the diamond roll. At this, the abrasive particles and the bonding at the circumference of the grinding wheel are crushed and the initial roughness reaches a maximum parameter. In contrast, at the ratio $q_d = 0$, the diamonds of the roll cause pronounced marks, which only cover each other slightly in axial direction. A high waviness appears in axial direction, which is the cause for the roughness increase [SCH73].

13.7.3 Conditioning of Super Hard Grinding Wheels

While profiling and dressing is carried out in one step with conventional grinding materials, super hard grinding wheels frequently require consecutively operated processes, because generally a sufficient exposure of abrasive particles concerning the bonding level of the grinding wheel cannot be achieved due to the profiling process [TÖN79].

The processes for profiling are partitioned into profiling tools, which can either contain diamonds or not (Fig. 13.44) [FRI99]. For the profiling of linear profiles, profiling with silicon carbide (SiC) roll is a common and economic process. The relative speed between profiling roll and grinding causes a mechanical abrasion. At this, the drive of the SiC roll occurs either by friction of the effective partners and is decelerated by means of a centrifugal force brake or the profiling unit possesses its own drive. In crushing, a steel or hard metal roll is deployed as a form or profile tool. The crushing roll is then pressed against the grinding wheel axially parallel and carried along by friction, at which no relative speed v_{rel} should occur between

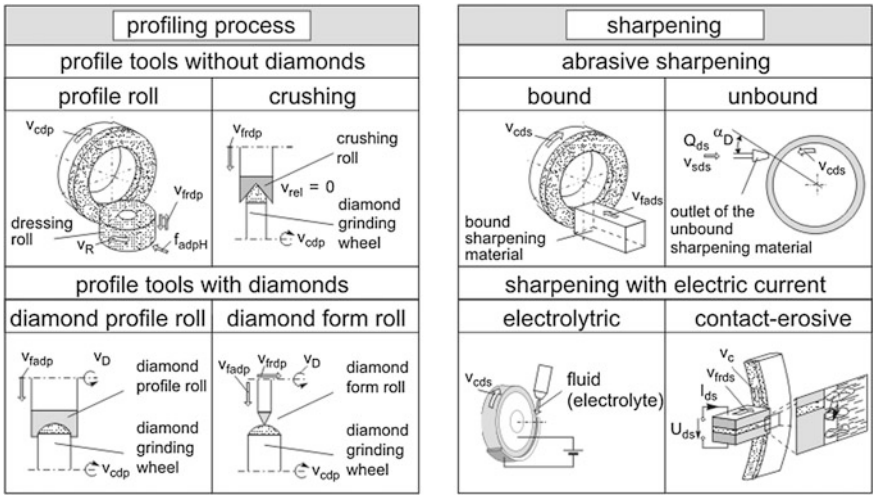

Fig. 13.44 Profiling and dressing processes for super hard grinding wheels

the effective partners. Vitrified or especially crushable (sufficiently brittle) metal bondings are necessary for this process. The use of tools containing diamonds allows a profile-representing (diamond profile roll) as well as a path-controlled (diamond form roll) profiling. Since the contact with the grinding wheel bonding reduces the durability of diamond dressing tools, it is generally recommendable to sharpen the grinding layer at the same time [TÖN75]. Point-crushing is a process, which is based on the engagement conditions of dressing with a form roll and the effective mechanisms of crushing. At this, the abrasive wear on the dressing tool is reduced by directing the relative speed between the effective partners towards zero or at least to a minimum.

Nowadays, rotating diamond dressing tools are increasingly used for the dressing of grinding wheels with vitrified bonding. The deployment of fixed dressing tools is irrelevant for super hard grinding wheels (especially diamond) due to the high wear. The dressing processes for super hard grinding wheels can be differentiated into abrasive processes and processes, which are based on the effect of electric current (Fig. 13.44).

The functional principle of dressing with a dressing block, also called block dressing, is based on the use of a bar-shaped dressing tool made of corundum or silicon carbide in vitrified or synthetic resin bonds. At this, the bonding material is set back due to the abrasive effect of the dressing material and the outermost abrasive particles are exposed.

In the so-called blast dressing process, a blasting material made of loose corundum or silicon carbide grain is blast onto the grinding surface with a bearing liquid (generally cutting liquid). At this, the targeted grain exposure occurs via the type and amount of dressing material as well as through the effective angle of the abrasive jet [UHL93].

Apart from the abrasive processes, dressing with electrolyte is becoming increasingly important for the dressing of very fine-grained diamond grinding wheels. For in-process dressing, it is called ELID-grinding [TIO90, OHM95]. The basic principle is based on the anodic ablation of bonding material in an electrolytic reaction. The grinding wheel, which is charged with a direct current via a brush system, represents the anode in this process. The gap between anode and cathode is filled with an electrolytic liquid and by means of the applied high-frequently pulsed operating current, electro-chemical ablation of the bonding material in the grinding layer takes place.

Another process based on the effect of electric current is contact erosion or electric erosion. The basic requirement for the deployment of dressing technology is an electrically-conductive bonding material. An electrode of conductive material, which is cut by the embedded grains, is fed to the grinding layer. Due to the applied stress, an electric field extends between the electrode and the grinding layer [FAL98], at which field distortions occur due to the cut electrode particles. Field exaggerations develop, which allow for a spark discharge between the electrode and the bonding material of the grinding wheels and, at this, cause a thermal ablation of the bonding material [FRI99].

Considering the timely order, we can differentiate between pre- and in-process dressing, i.e., the dressing takes place at the same time as the grinding process. The effects of the in-process dressing by means of a dressing block are illustrated in Fig. 13.45 in the machining of ceramic. The dressing process without the deployment of in-process dressing technology is characterised by increasing dressing forces, which can be attributed to the effective wear mechanisms such as clogging and grain blunting.

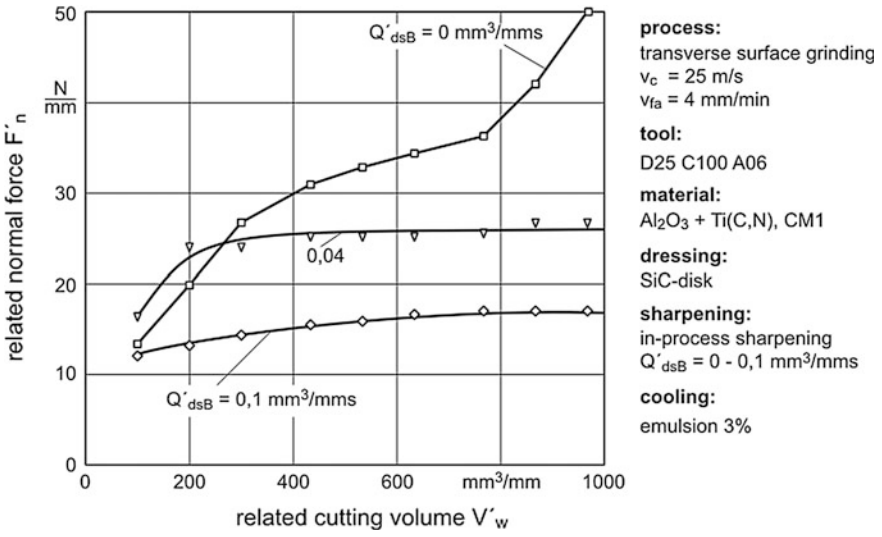

Fig. 13.45 Influence of the block dressing material removal rates Q_{dsB} on the process course

The use of in-process block dressing can minimise the influences of the wear mechanisms. Depending on the selected block dressing material removal rate Q_{dsB}, stationary dressing force courses develop after an infeed phase. An increase of Q_{dsB} and thus an increase of the dressing intensity lead to a reduction of the dressing force level.

13.8 Grinding Costs

Grinding is a "twin process", i.e., apart from the actual grinding process, the dressing also has to be considered regarding the costs.

The grinding costs per unit are then

$$K_F = K_{mach} + K_T + K_d \tag{13.72}$$

with

K_{mach} machine costs incl. wages (space costs)
K_T costs of grinding tool per piece
K_d costs for dressing calculated per piece.

The machine costs result from the machine time rate plus labour costs [TÖN95] (space costs per time unit k_{sp}) and the total time $t_{tot.} = t_h + t_n$ from main and secondary time [DEN10]

$$K_{mach} = k_{sp} \times (t_h + t_n) \tag{13.73}$$

The main time/operating time t_h can be detected via the radial feed speed (in plunge grinding) and the oversize or from the volume to be ground V_w and the material removal rate Q_w. Subsequently, the wheel volume worn during the grinding process V_s results from the grinding ratio $G = V_w/V_s$ defined above

$$K_T = V_s \times k_s \tag{13.74}$$

with the wheel costs per volume unit k_s. Then the dressing costs K_d are added. These are

$$K_d = (k_{pl} \times t_{tot,d} + V_{s,d} \times k_d)/n + K_{T,d}/n \tag{13.75}$$

with the total dressing time $t_{tot,d}$, the wheel volume lost by dressing $V_{s,d}$, and the dressing material worn due to the dressing $K_{T,d}$. To collect the proportion falling upon one piece, we must divide by the quantity n, that means by the number of pieces up to the next dressing cycle.

Example: Plunge grinding of a shaft of tempered steel 42CrMoV4 with diameter $d = 30$ mm, grinding width $a_p = 20$ mm and grinding oversize $w = 0.25$ mm at a tolerance width of 10 µm. Grinding is carried out with corundum (k_s = Euro 100 10^{-6}/mm^3, $G = 40$) and, due to the required accuracy,

in a two-step operation (roughing at $v_{fr} = 1.5$ mm/min, finishing at $v_{fr} = 0.25$ mm/min) The wheel life quantity up to the dressing is to be 15 pieces.

Together with practical data, the following costs result per workpiece:

$K_F = 4.10$ € with the portions: $K_{mach}/K_F = 0.90$, $K_T/K_F = 0.08$, $K_d/K_F = 0.02$.

If the same task is machined with a super hard grinding wheel on CBN basis, the cost for the tool rises to approx. 15 %, the grinding time and thus the machine-dependent costs K_{mach} decrease, possibly over-proportionally less.

13.9 Questions

1. Name processes, which cut with undetermined cutting edges.
2. Classify the processes according to their separating mechanisms and the effective motion.
3. Do you see limitations for the path bonding during the grinding process? How do you explain the energy bonding in the blast cutting process?
4. Which grinding processes do you know? Name the corresponding motions of tool and workpiece.
5. Deduce the equivalent cutting thickness h_{eq} from the continuity condition.
6. Indicate the equivalent diameter for different grinding processes.
7. Which components is a grinding wheel composed of? What tasks do they have?
8. Which grinding materials do you know? Organise them according to their hardness.
9. Which deployment areas do you assign to the grinding materials?
10. What does the friability index mean? Which material properties does it characterise?
11. How is the friability index determined?
12. Which kinds of corundum grinding materials do you know? How are they structured and what effect is achievable with them?
13. Characterise the possible crystal shapes of the super hard grinding materials. What does the index 111 mean? And what about 100?
14. How is the grain size of a grinding material specified and how is it determined?
15. What is meant with the hardness of a grinding wheel? How can it be influenced?
16. How can the hardness of a grinding wheel be determined?
17. Which types of bonding do you know?
18. How can the wear of a grinding wheel be defined?
19. How can the average radius wear of a wheel be calculated from the G parameter (grinding ratio)?
20. Which loads are dominant in the case of fast-running grinding wheels? Where is the maximum load?

21. What basic equations does one need to determine the dominant load of a grinding wheel by calculation?
22. How are the blasting speed and the permitted operating speed connected?
23. What possibilities do you see to increase the bursting speed resp. the permitted work speed?
24. What advantage does a holeless grinding wheel have (theoretically)?
25. Which types of wear occur at the grinding wheel?
26. Characterise the grinding process in the sense of the system technology (black-box).
27. Name the characteristics for the description of grinding processes.
28. What is the purpose of the equivalent radius?
29. What is not considered by the approximate calculation for the geometric contact length?
30. How do the kinematic and the geometric contact length differ?
31. How can the average cutting thickness in the grinding process by deduced considering the micro-topography of the grinding wheel?
32. Give an estimate as to how the energy removal from the grinding zone adjusts with different grinding materials.
33. Which methods for temperature measurement in the grinding process do you know?
34. What does the term conditioning of grinding wheels include? Name the tasks of the single process steps.
35. Divide the dressing processes and name typical dressing tools.
36. Which dressing processes do you apply for small, medium and large series?
37. What effect do you achieve by dressing in the same or counter direction?
38. How is the degree of overlapping defined in the dressing process; how and when does it affect the roughness at the workpiece and the forces in the grinding process?
39. Name dressing processes and subdivide them according to their effective principle.
40. Indicate the most important terms for the cost calculation in the grinding process.

References

[ANSB7418] American National Standard B 7418–1965: Ball Mill Test of Friability of Abrasive Grains

[ARG00] Argyropoulos, G.: Rundschleifen mit Schleifbändern, Schleiftechnik im Wettbewerb [External grinding by abrasive belts, grinding technology in competition]. 2. Schleiftechnisches Kolloquium, November 2000, Bremen

[BRI82] Brinksmeier, E.: Randzonenanalyse geschliffener Werkstücke [Surface zone analysis of ground workpieces]. Dr.-Ing. Diss. Universität Hannover 1982

[BRI91] Brinksmeier, E.: Prozess- und Werkstückqualität in der Feinbearbeitung [Process- and workpiece-quality in fine finishing]. Habilitationsschrift, Universität Hannover (1991)

[BRU98] Brunner, G: Schleifen mit mikrokristallinen Aluminiumoxid Schleifkorn [Grinding by micro-cristalline alumina grains]. Dr.-Ing. Diss. Universität Hannover (1998)

[BUN55] Bundy, F.P., Hall, H.T., Strong, H.M., Wentorf, R.F.: Man-made diamonds. Nature **176**, S.55 (1955)

[BÜT68] Büttner, A.: Das Schleifen sprödharter Werkstoffe mit Diamant-Topfscheiben [The grinding of brittle materials by diamond cup wheels]. Dr.-Ing. Diss. Universität Hannover (1968)

[CHO86] Choi, H.Z.: Beitrag zur Ursachenanalyse der Randzonenbeeinflussung beim Schleifen [Contribution to cause analysis of surface integrity in grinding]. Dr.-Ing. Diss. Universität Hannover (1986)

[COL81] Colleselli, K.: Konventionelle Schleifmittel und Bindungen zur Herstellung von Schleifkörpern [Conventional abrasives and bonds to manufacture grinding wheels]. Jahrbuch Schleifen, Honen, Läppen und Polieren, 50. Ausgabe, S. 207–211 (1981)

[CZE99] Czenkusch, C.: Technologische Untersuchungen und Prozessmodelle zum Rundschleifen [Technological investigations and process models for external grinding]. Dr.-Ing. Diss. Universität Hannover (1999)

[DEN03] Denkena, B., Becker, J.C., Catoni, F.: Characterisation of vitrified bonded grinding wheels. ISAAT, Bristol, 18–20 Nov (2003)

[DEN10] Denkena, B.: Konstruktion, Gestaltung und Herstellung von Produkten II. Vorlesungsmanuskript [Design, configuration and manufacturing of products II, lecture manuscript]. Universität. Hannover (2010)

[DIN8589-0] Fertigungsverfahren Spanen—Teil 0: Allgemeines; Einordnung, Unterteilung, Begriffe/Manufacturing processes chip removal—Part 0: General; classification, subdivision, terms and definitions. Hrsg. Beuth Verlag (2003)

[DIN ISO8486-1] Schleifkörper aus gebundenem Schleifmitel—Bestimmung und Bezeichnung von Korngrößenverteilung—Teil 1: Makrokörnungen F4 bis F220/Bonded abrasives—Determination and designation of grain size distribution—Part 1: Macrogrits F4 to F220. Hrsg. Beuth Verlag (1997)

[DIN ISO 525] Schleifkörper aus gebundenem Schleifmittel - Allgemeine Anforderungen/ Bonded abrasive products – General requirements. Hrsg. Beuth Verlag (2000)

[DOW72] Dow Whitney, E.: Thermodynamic properties of abrasive materials. In: Proceedings of International Grinding Conference, Pittsburg (1972)

[FAL98] Falkenberg, Y.: Elektroerosives Schärfen von Bornitrid Schleifscheiben [Electro-erosive dressing BN grinding wheels]. Dr.-Ing. Diss. Universität Hannover (1998)

[FRI02] Friemuth, T.: Herstellung spanender Werkzeuge [Production of cutting tools]. Habilitation, Universität Hannover (2002)

[FRI99] Friemuth, T.: Schleifen hartstoffverstärkter Werkzeuge [Grinding of hard particle reinforced tools]. Dr.-Ing. Diss. Universität Hannover (1999)

[GRA87] Grabner, T.: Leistungspotenial keramisch gebundener CBN-Schleifscheiben [Power potential of CBN grinding wheels]. Dr.-Ing. Diss. Universität Hannover (1987)

[GRE58] Greiner, K.: Festigkeitsuntersuchungen an Klebeverbindungen zwischen Schleif- und Tragkörper [Investigation of strength at glued connections between wheel and carrying body]. Dr.-Ing. Diss. TH Hannover (1958)

[HAU80] Hauk, V.; Krug, W.K.; Vaessen, G; Weisshaupt; H.: Der Eigendehnungs-/ Eigenspannungszustand nach Schleifbeanspruchung [the residual strain/ residual stress state after grinding loadst]. HTM **35**(3), S. 61–62 (1980)

[HAH63] Hahn, R.S.: On the nature of the grinding process. In: Proceedings Third International MTDR Conference, Sept. 1962, Oxford, S.129–154 (1963)

[HAL60] Hall, H.T.: Ultra high pressure temperature analysis. The belt. Rev. Sci. Inst. 31, 125, (1960)

[HEU92] Heuer, W: Außenrundschleifen mit kleinen CBN-Scleifscheiben [External grinding with small wheels]. Dr.-Ing. Diss. Universität Hannover (1992)

[KAI75] Kaiser, M.: Schleifen von Hartmetallen [Grinding of cemented carbides]. Dr.-Ing. Diss. TU Hannover 1975, München: Techn. Verlag Resch (1975)

[KAI09] Dr. Kaiser GmbH: Company booklet. Celle (2009)

[KAR95] Karpuschewski, B.: Mikromagnetische Randzonenanalyse geschliffener einsatzgehärteter Bauteile [Micro-magnetic analysis of surface zones of ground case hardened components]. Dr.-Ing. Diss. Universität Hannover (1995)

[KAR01] Karpuschewski, B.: Sensoren zur Prozessüberwachung beim Spanen [Sensors for process monitoring in cutting]. Habilitation, Universität Hannover (2001)

[KAS69] Kassen, G.: Beschreibung der elementaren Kinematik des Schleifvorganges [Description of the elementary kinematics oft he grinding process]. Dr.-Ing. Diss. RWTH Aachen (1969)

[KEL80] Kelker, H.(Hrsg.): Ullmanns Encyklopedie der technischen Chemie [Encyclopedia of technical chemestry]. 4. neubearbeitete und erweiterte Auflage, Band 5 Analysen und Messverfahren. Verlag Chemie, Weinheim (1980)

[KLO02] Klocke, F., Merbecks, T.: Charakterisierung von keramisch gebundenen CBN-Scleifscheiben [Characterization of vitrified bond CBN grinding wheels]. IDR 36 Nr. 3, S. 242–251 (2002)

[KLO86] Klocke, M.: Einfluss des Gefüges von Edelkorund Schleifscheiben auf ihre Werkstoffkennwerte und das Schleifverhalten [Influence of the structure of aluminum oxide grinding wheels on their material parameters and their grinding behavior]. Dr.-Ing. Diss. TU Berlin (1986)

[KUR27] Kurrein, M.: Die Bearbeitbarkeit der Metalle im Zusammenhang mit der Festigkeitsprüfung [Machinability of metals regarding the strength test]. Werkstattechnik **21**, S.612–621 (1927)

[LIE98] Lierse, T.: Mechanische und thermische Wirkungen beim Schleifen keramischer Werkstoffe [Mechanical and thermal effects in grinding of ceramic materials]. Dr.-Ing. Diss. Universität Hannover (1998)

[LOR75] Lortz, W.: Schleifscheibentopographie und Spanbildungsmechanismen beim Schleifen [Grinding wheel topography end chip formation mechanisms in grinding]. Dr.-Ing. Diss. RWTH Aachen (1975)

[MAH00] Mahoney, M.: Höhere Zerspanleistung durch neue Schleifscheibenstrukturen [Higher material removal rates by new grinding wheel structures]. Schleiftechnik im Wettbewerb, 2. Schleiftechnisches Kolloquium, November 2000, Bremen

[MAG08] Malkin, S., Guo, C.: Grinding technology. Industrial Press, New York (2008)

[MAR01] Marzenell,C.: Verzahnungshonen mit Diamantwerkzeugen [Gear honing with diamond tools]. Dr.-Ing. Diss. Universität Hannover (2001)

[MIN99] Minke; E.: Handbuch zur Abrichttechnik [Handbook of dressing technology]. Eislingen, Druck und Verlag E. Dischner

[MÜL01] Müller, N.: Ermittlung des Einsatzverhaltens von Sol-Gel-Korund Schleifscheiben [Determination oft he application behavior of sol-gel carborundum grinding wheels]. Dr.-Ing. Diss. RWTH Aachen (2001)

[OHM95] Ohmori, H.: Ultraprecision grinding of optical materials and components applying ELID (Elektrolytic In-Process Dressing). SPIE **2576**, S. 26–45 (1995)

[PAD93] Padberg, H.-J.: Entwicklung anwendungsorientierter Bindungs-Systeme für Schleifwerkzeuge [Development of application related bond systems for

grinding tools]. Jahrbuch Schleifen, Honen, Läppen und Polieren, 57. Ausgabe, S. 196–211 (1993)

[PAU94] Paul, T.: Konzept für ein schleiftechnologisches Informationssystem [Concept for a grinding technological information system]. Dr.-Ing. Diss. Universität Hannover (1994)

[PEK57] Peklenik, J.: Ermittlung von geometrischen und physikalischen Kenngrößen [Determination of geometric and physical characteristics]. Dr.-Ing. Diss. RWTH Aachen (1957)

[PET68] Peters, J., Snoeys, R., Decnent, A.: Sonic testing of grinding. In: Proceedings of 9th International Machine Tool Design and Research Conference, S.1113 (1968)

[RAM78] Ramdohr, P.; Strunz, H.: Klockmanns Lehrbuch der Mineralogie [Textbook of mineralogy]. Ferdinand Enke Verlag, Stuttart (1978)

[REI56] Reichenbach, G.S., Mayer, J.E., Shaw, M.C., et al.: The role of chip thickness in grinding. Trans. ASME **78**, S.847–859 (1956)

[ROT94] Roth, P.: Abtrennmechanismen beim Schleifen von Aluminiumoxidkeramik [Cutting mechanisms in grinding of aluminum oxide]. Dr.-Ing. Diss. Universität Hannover (1994)

[ROW93] Rowe, W.B. et al.: The effect of deformation on the contact area in grinding. Ann. CIRP **42**(1), S.409–412 (1993)

[SAL82] Salmang, H.; Scholze H.: Keramik [Ceramics]. Springer Verlag 6. Aufl. (1982)

[SAL91] Saljé, E.: Begriffe der Schleif- und Konditioniertechnik. Essen, Vulkan Verlag (1991)

[SCH68] Schmitt, R.: Abrichten von Scheifscheiben mit diamantbestückten Rollen [Dressing of grinding wheels by bediamonded rolls]. Dr. -Ing. Diss. TU Braunschweig (1968)

[SCH73] Scheidemann, H.: Einfluss der durch Abrichten mit zylindrischen und profilierten Diamantrollen erzeugten Schleifscheiben-Schneidfläche auf den Schleifvorgang [Influence of the grinding wheel cutting face, generated by cylindric and profiled diamond rolls]. Dr.-Ing. Diss. TU Braunschweig (1973)

[SIM88] Simpfendörfer, D.: Entwicklung und Verifizierung eines Prozessmodells beim Planparallelläppen [Development and verification of a process model in double plate face lapping]. Dr.-Ing. Diss. TU Berlin (1988)

[SPU89] Spur, G.: Keramikbearbeitung [Machining of ceramics]. München: Carl Hanser Verlag (1989)

[STA62] Stade, G.: Technologie des Schleifens [Technology of grinding]. München, Carl Hanser Verlag (1962)

[STA02] Stabenow, R.; Bruhn, J.; Golla, B. J.: Mikrokristalline Sinterkeramik in Schleifkörpern [Micro-cristalline sintered ceramic in grinding wheels]. 10. Internationales Braunschweiger Feinbearbeitungskolloquium, Braunschweig (2002)

[TIO90] Tio, T.-H.: Pendelschleifen nicht oxidischer Keramiken [Reciprocating grinding of non-oxidi ceramics]. Dr.-Ing. Diss. TU Berlin (1990)

[TÖN65] Tönshoff, H.K.: Eigenspannungen und plastische Verformungen im Werkstück durch spanende Bearbeitungsverfahren [Residual stresses and plastic deformations in the workpiece by cutting and abrasive processes]. Dr.-Ing. Diss. TH Hannover (1965)

[TÖN75] Tönshoff, H.K.; Kaiser, M.: Profilieren und Abrichten von Diamant- und Bornitrid-Schleifscheiben [Profiling and dressing of diamond and boron nitride grinding wheels]. wt-Z.ind.Fertig. 65(1975)4, S. 179–183, (1975)

[TÖN79] Tönshoff, H.K., Geisweid, G.: Profiling of diamond and boron nitride wheels. Ann. CIRP **28**, 1 (1979)

[TÖN92] Tönshoff, H.K. et al.: Modelling and simulation of grinding process. Ann. CIRP **41**(2) S.677–688 (1992)

[TÖN95] Tönshoff, H.K.: Werkzeugmaschinen- Grundla gen [Machine tools—fundamentals]. Springer (1995)

[TRI76] Triemel, J.: Untersuchungen zum Stirnschleifen von Schnellarbeitsstählen mit Bornitridwerkzeugen [Investigations of face grinding of high speed steels by boron nitride tools]. Dr.-Ing. Diss. Universität Hannover (1976)

[UHL87] Uhlmann, E; Stark, C.: Potentiale von Schleifwerkzeugen mit mikrokristalliner Aluminiumoxidkörnung [Potentials of grinding tools with micro-cristalline aluminum oxide grains]. Jahrbuch Schleifen, Honen, Läppen und Polieren **58**, S. 281–309 (1987)

[UHL93] Uhlmann, E.: Tiefschleifen hochfester keramischer Werkstoffe [Creep grinding of high strength ceramic materials]. Dr.-Ing. Diss. TU Berlin (1993)

[VER79] Verkerk, J., Pekelharing, A.J.: The influence of the dressing operation on productivity in precision grinding. Ann. CIRP **28**, 2 (1979)

[VOL00] Vollstädt, H.; List, E.; Recht, H.: Methoden und Geräte zur Qualitätsbestimmung von Industriediamanten [Methods and devices to determine the quality of industrial diamonds]. Poceedings of 4. IFW-Steinseminar, 4–6.7.2000, Seite 43–52

[WEI76] Weinert, K.: Die zeitliche Änderung des Schleifscheibenzustandes beim Außenrund-Einstechschleifens [The temporal alteration of the grinding wheel state in external grinding]. Dr.-Ing. Diss. TU Braunschweig (1976)

[WER71] Werner, G.: Kinematik und Mechanik des Schleifprozesses [Kinematic and mechanics of the grinding process]. Dr.-Ing. Diss. RWTH Aachen (1971)

[WOB91] Wobker, H.-G.: Schleifen keramischer Werkstoffe [Grinding of ceramic materials]. Dr.-Ing. Diss. Universität Hannover (1991)